En-gauging Naturalness

Aoife Bharucha,[a,b] **Andreas Goudelis**[c] **and Moritz McGarrie**[d]

[a] *II. Institut für Theoretische Physik, Universität Hamburg, Luruper Chaussee 149, D-22761 Hamburg, Germany*

[b] *Physik Department T31, Technische Universität München, James-Franck-Straße 1, D-85748 Garching, Germany*

[c] *LAPTh, Université de Savoie, CNRS, 9 Chemin de Bellevue, B.P. 110, F-74941 Annecy-le-Vieux, France*

[d] *Deutsches Elektronen-Synchrotron, DESY, Notkestrasse 85, D-22607 Hamburg, Germany*

E-mail: aoife.bharucha@tum.de, andreas.goudelis@lapth.cnrs.fr, moritz.mcgarrie@desy.de

ABSTRACT: The discovery of a 125.5 GeV Higgs with standard model-like couplings and naturalness considerations motivate gauge extensions of the MSSM. We analyse two variants of such an extension and carry out a phenomenological study of regions of the parameter space statisfying current direct and indirect constraints, employing state-of-the-art two-loop RGE evolution and GMSB boundary conditions. We find that due to the appearance of non-decoupled D-terms it is possible to obtain a 125.5 GeV Higgs with stops below 2 TeV, while the uncolored sparticles could still lie within reach of the LHC. We compare the contributions of the stop sector and the non-decoupled D-terms to the Higgs mass, and study their effect on the Higgs couplings. We further investigate the nature of the next-to lightest supersymmetric particle, in light of the GMSB motivated searches currently being pursued by ATLAS and CMS.

Contents

1 Introduction

The recent discovery of a ~ 125.5 GeV particle consistent with the properties of the standard model Higgs boson [1, 2] and no direct evidence of supersymmetry (SUSY) in the current LHC data are pushing traditional setups of gauge-mediated supersymmetry breaking (GMSB) for the minimal supersymmetric standard model (MSSM) into fine-tuned territory. In the MSSM, to obtain a lightest CP-even scalar of the observed mass requires either heavy stops, thereby introducing a *naturalness* or fine-tuning problem, or substantial left-right stop mixing, which, being strongly dependent on the trilinear soft term A_t, is heavily influenced by the mechanism of supersymmetry-breaking mediation that is invoked. In particular, in GMSB trilinear terms such as A_t are vanishing at the supersymmetry breaking scale M, and a large A_t can only be generated via renormalisation group evolution. This requires the scale M to be very high, which is also detrimental to the naturalness of the theory. Moreover, in minimal SUSY models, choosing heavy stops results in the sparticle spectrum becoming heavier and beyond the reach of the LHC, and consequently phenomenologically less interesting.

The heart of the problem appears to be that in the MSSM, the tree-level Higgs mass is simply too small, the upper bound being the mass of the Z boson. If however we drop minimality from our criteria, natural scenarios of supersymmetry breaking *with* discovery potential still persist. These usually involve lifting the Higgs potential at tree-level through non-decoupled F or D type terms [3, 4], which arise when the MSSM is extended by additional gauge groups. The less-studied gauge extensions involving non-decoupled D-terms could enhance the tree-level Higgs mass, result in detectable deviations in the Higgs couplings, and further induce suppressions to the scalar masses compared to minimal GMSB. Such models may therefore have a direct impact on phenomenology and, unsurprisingly, have of late found increasing interest [5–11].

In this paper we study a quiver model or gauge extension of the MSSM within the framework of GMSB, to determine whether it is indeed possible to reproduce the observed Higgs boson mass while keeping the stop masses below roughly 2 TeV. In particular we build a tailor-made spectrum generator for our model using the publicly available tool SARAH. This allows us to perform the renormalization group evolution at two loops and analyze several aspects of the model's phenomenology. Although we do not carry out a thorough "naturalness" or fine-tuning study, it is at least clear that qualitively, having stops lighter than benchmark minimal GMSB certainly improves the relative naturalness of the model. We therefore study the resulting spectra for the model, consistent with experimental results, in particular the Higgs sector. We further investigate possible signatures of this model at the LHC, taking into account the latest results of GMSB motivated searches.

The outline of the paper is as follows: In section 2 we give a first account of our key findings. In section 3 we present the specific realization of a quiver gauge theory that we will be studying in the following sections, discuss its general features and our choice of parameterisation of the soft term boundary conditions. Amusingly, these setups in some sense also model the effects of a truncated theory of gauge fields in an extra dimension [7, 12] and we make a small digression in section 3.5 to discuss this connection. In section
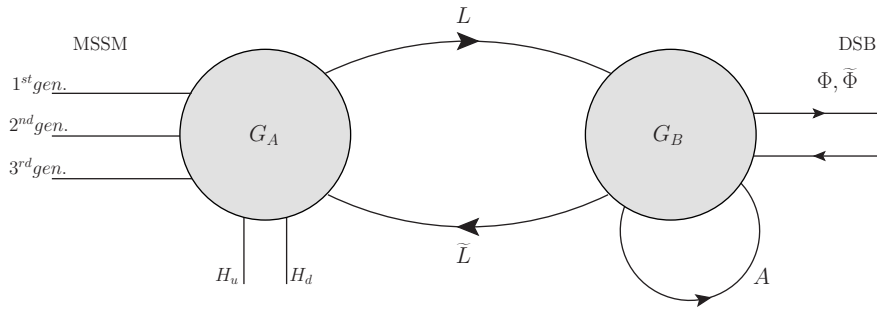
Figure 1. A picture to represent the quiver module of the electroweak sector for MI as in table 2. The electroweak part of the supersymmetric standard model is on site A, with messenger fields $(\Phi, \tilde{\Phi})$ coupled to another site, site B. The linking fields $(L, \tilde{L})$ connect the two sites. The adjoint field (A) is charged on the second site, site B. The singlet field (K) is not shown.

4 we discuss the concrete implementation of our quiver setup, the model's parameter space and the phenomenological constraints it is subject to. Then, in section 5 we present our results on the phenomenology of the model and discuss the features of its particle spectrum. Finally, in section 6 we conclude. The appendix A contains details about the implementation of our framework along with some important relations. This paper is accompanied by a supplementary document containing details with regards to the implementation [13].

2 Key results

It is useful here to give a first summary of our key results. In this work we will show that

- With the setup we adopt it is perfectly possible to obtain a 125.5 GeV Higgs with stops lighter than 2 TeV, gluinos of order 1600 GeV, light electroweakinos and sleptons potentially within the reach of the LHC, all within a GMSB framework (see benchmarks in table 5).

- The correct Higgs mass is obtained through *non decoupled D-term* contributions in the low-energy lagrangian that lift the Higgs boson mass at tree level, as shown in figure 4.

- These terms also modify the Higgs branching ratios but well within current LHC bounds, and could be probed by the ILC as seen in figure 6.

- The light uncoloured sparticle spectrum is achieved primarily due to the specific supersymmetry breaking mediation mechanism we employ (see figure 7).

These results are obtained by implementing our model into the publicly available package `SARAH`, which enables us to create a spectrum generator in order to perform the RGE evolution of all model parameters at two loops, from the messenger scale M down to the TeV scale, with GMSB boundary conditions.

SF	Spin $\frac{1}{2}$	Spin 1	$SU(N)$	Coupling
$\hat{B}_A$	$\tilde{B}_A$	B_A	$U(1)_A$	g_{A1}
$\hat{W}_B$	$\tilde{W}_B$	W_B	$SU(2)_B$	g_{B2}
$\hat{g}$	$\tilde{g}$	g	$SU(3)_c$	g_3
$\hat{B}_B$	$\tilde{B}_B$	B_B	$U(1)_B$	g_{B1}
$\hat{W}_A$	$\tilde{W}_A$	W_A	$SU(2)_A$	g_{A2}

Table 1. Gauge superfields of the model.

We have implemented five gauge groups at full one- and two-loop running, plus one-loop self energies, from the GUT or messenger scale, Higgsing and breaking to the diagonal subgroup of 4 gauge groups, while finite shifts and threshold corrections are carefully applied for each degree of freedom.

We finally stress that we have implemented a conservative (precise) formulation of GMSB with full two loop equations for soft masses in the hidden sector. Still at this level of specification a reasonably natural spectrum is obtained, which demonstrates the ease with which much lighter spectra would be obtainable if these high standards were relaxed or some more phenomenological parameterisation adopted. The framework that we have developed quite straightforwardly admits numerous extensions such as inclusion of $U(1)$ kinetic mixing or quivering the $SU(3)$ sector, tasks which are left for future work. All of these remarks will be clarified in the following sections.

3 An electroweak quiver

In this paper we wish to explore two different quiver models for comparison. The first carries the generic features of non-decoupled D-terms and, in the case of GMSB, suppressed scalar soft masses versus gauginos. The second is a flavourful extension of the first model to achieve lighter stops than the first two generations, which still obeys all anomaly cancellations. A common feature is that we will apply a gauge mediated supersymmetry breaking scenario to both and both are characterised by the scale of supersymmetry breaking, M, and the vevs of the linking fields[1], v. In this section we outline these models and their features.

3.1 The models and features

Let us consider an electroweak two-site quiver with gauge group $G_A \times G_B \times SU(3)_c$, where $G_A = SU(2)_A \times U(1)_A$ and $G_B = SU(2)_B \times U(1)_B$ as in table 1. The two sites are connected by means of a pair of linking chiral superfields $\hat{L}$, $\hat{\tilde{L}}$. These superfields will play a crucial role both in the breaking of the enlarged gauge group to the MSSM gauge groups, by obtaining vevs, and in the mediation of supersymmetry breaking effects. Moreover, the setup includes a singlet chiral superfield K, whose role will be clarified shortly, as well as

---

[1]not to be confused with v_{ew}.

SF	Spin 0	Spin $\frac{1}{2}$	$G_A \times G_B \times SU(3)_c$ (MI)
$\hat{q}^f$	$\tilde{q}^f$	q^f	$(\mathbf{2}, \frac{1}{6}, \mathbf{1}, 0, \mathbf{3})$
$\hat{l}^f$	$\tilde{l}^f$	l^f	$(\mathbf{2}, -\frac{1}{2}, \mathbf{1}, 0, \mathbf{1})$
$\hat{H}_d$	H_d	$\tilde{H}_d$	$(\mathbf{2}, -\frac{1}{2}, \mathbf{1}, 0, \mathbf{1})$
$\hat{H}_u$	H_u	$\tilde{H}_u$	$(\mathbf{2}, \frac{1}{2}, \mathbf{1}, 0, \mathbf{1})$
$\hat{d}^f$	$\tilde{d}_R^{f*}$	d_R^{f*}	$(\mathbf{1}, \frac{1}{3}, \mathbf{1}, 0, \overline{\mathbf{3}})$
$\hat{u}^f$	$\tilde{u}_R^{f*}$	u_R^{f*}	$(\mathbf{1}, -\frac{2}{3}, \mathbf{1}, 0, \overline{\mathbf{3}})$
$\hat{e}^f$	$\tilde{e}_R^{f*}$	e_R^{f*}	$(\mathbf{1}, 1, \mathbf{1}, 0, \mathbf{1})$
$\hat{L}$	L	ψ_L	$(\mathbf{2}, -\frac{1}{2}, \overline{\mathbf{2}}, \frac{1}{2}, \mathbf{1})$
$\hat{\tilde{L}}$	$\tilde{L}$	$\psi_{\tilde{L}}$	$(\overline{\mathbf{2}}, \frac{1}{2}, \mathbf{2}, -\frac{1}{2}, \mathbf{1})$
$\hat{K}$	K	ψ_K	$(\mathbf{1}, 0, \mathbf{1}, 0, \mathbf{1})$
$\hat{A}$	A	ψ_A	$(\mathbf{1}, 0, \mathbf{3}, 0, \mathbf{1})$

Table 2. Chiral superfields of the model MI. The index f runs over all three generations. The representation ordering corresponds to $(SU(2)_A, U(1)_A, SU(2)_B, U(1)_B, SU(3)_c)$. The superpotential is Eqn. (3.1) and Eqn. (3.2) and the supersymmetry breaking messenger fields are charged under site B.

an additional superfield A transforming as the adjoint of $SU(2)_B$ that serves the role of giving masses to certain fermionic components of the linking fields upon $G_A \times G_B$ breaking. Much below the higgsing scale, v, the quiver fields usually decouple and so for phenomenological purposes at low energies the model is essentially MSSM-like with the addition of an effective action for the Higgs potential. It will be useful then to refer to the enlarged gauge groups as regime 1 and the MSSM as regime 2. This paper is based on two models which are as follows:

[**Model I**]: The first model (MI) is a basic example of a quiver model where the MSSM chiral superfields are taken to be charged under site A identically to their charges under the MSSM gauge group and are neutral under site B (see figure 1 and table 2). The superpotential of the MSSM-like matter is given by

$$W_{\text{SSM}} = Y_u \, \hat{u} \, \epsilon_{ij} \hat{q}^i \, \hat{H}_u^j - Y_d \, \hat{d} \, \epsilon_{ij} \hat{q}^i \, \hat{H}_d^j - Y_e \, \hat{e} \, \epsilon_{ij} \hat{l}^i \, \hat{H}_d^j + \mu \epsilon_{ij} \, \hat{H}_u^i \, \hat{H}_d^j \qquad (3.1)$$

with i, j, k labelling $SU(2)$ indices, and as this group is pseudo real, the $\overline{\mathbf{2}}$ ϕ_i is simply $\epsilon_{ij} \phi^j$ of the 2 representation ϕ^i of $SU(2)$. The superpotential of the quiver module is given by

$$W_{\text{Quiver}} = \frac{Y_K}{2} \hat{K} (\hat{L}_i^j \, \hat{\tilde{L}}_j^i - V^2) + Y_A \, \hat{L}_i^j \, \hat{A}_j^k \, \hat{\tilde{L}}_k^i . \qquad (3.2)$$

The general features of this model will be outlined below and unless stated in the text all RGEs and equations of this paper refer to MI.
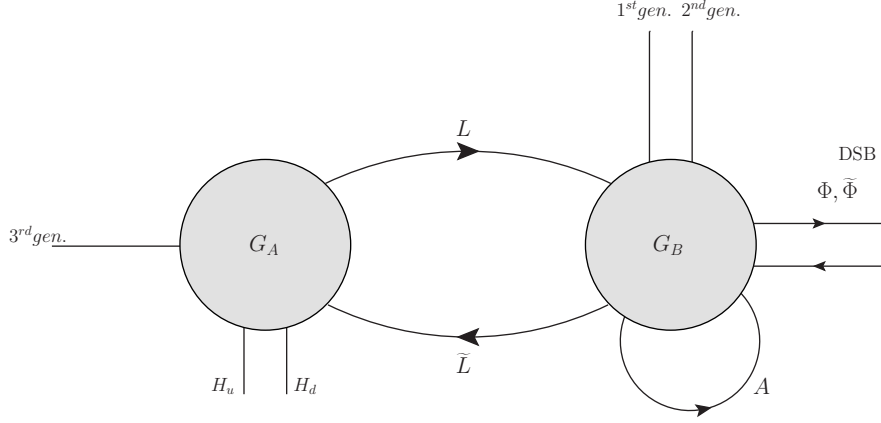
Figure 2. The quiver module of the electroweak sector for MII as in table 3. The first and second generation matter is charged under site B and the third generation and MSSM Higgs fields are charged under site A. The messenger fields $(\Phi, \tilde{\Phi})$ are charged under site B. The linking fields $(L, \tilde{L})$ connect the two sites.

[**Model II**]: The second model (MII) is a flavourful deformation of model I in that by construction the first and second generation MSSM chiral superfields are taken to be charged under site B and neutral under site A while the 3rd generation and the Higgs fields are kept on site A (see figure 2 and table 3). The superpotential we use in regime 1 is

$$W_{\mathrm{MII}} = Y_u^3\, \hat{u}^3\, \epsilon_{ij}\hat{q}^{3i}\, \hat{H}_u^j - Y_d^3\, \hat{d}^3\, \epsilon_{ij}\hat{q}^{3i}\, \hat{H}_d^j - Y_e^3\, \hat{e}^3\, \epsilon_{ij}\hat{l}^{3i}\, \hat{H}_d^j + \mu\, \epsilon_{ij}\hat{H}_u^i\, \hat{H}_d^j \qquad (3.3)$$

plus the quiver superpotential Eqn. (3.2). In regime 2 after returning to the MSSM gauge groups, we adopt the MSSM superpotential by Eqn. (3.1).

3.2 Gauge symmetry breaking

We now describe certain features of the general setup. The superpotential Eqn. (3.2) gives rise to a scalar potential which when minimized sets a vacuum expectation value for the scalar components of the linking fields of the model. Denoting

$$L = \begin{pmatrix} \varphi_{L1} & \varphi_{L2} \\ \varphi_{L3} & \varphi_{L4} \end{pmatrix} \qquad (3.4)$$

we write

$$\langle L \rangle = \langle \tilde{L} \rangle = v\mathbb{I}_{2\times 2} \quad \text{where} \quad \mathrm{tr}(v^2\mathbb{I}_{2\times 2}) = V^2. \qquad (3.5)$$

These break the gauge group $G_A \times G_B$ down to the diagonal subgroup $G_{\mathrm{Diag}} = SU(2)_L \times U(1)_Y$, which are simply the MSSM gauge groups. The symmetry breaking pattern takes the form

$$SU(2)_A \times SU(2)_B \to SU(2)_L \quad \text{and} \quad U(1)_A \times U(1)_B \to U(1)_Y. \qquad (3.6)$$

SF	Spin 0	Spin $\frac{1}{2}$	$G_A \times G_B \times SU(3)_c$ (MII)
$\hat{q}^{1,2}$	$\tilde{q}^{1,2}$	$q^{1,2}$	$(\mathbf{1}, 0, \mathbf{2}, \frac{1}{6}, \mathbf{3})$
$\hat{l}^{1,2}$	$\tilde{l}^{1,2}$	$l^{1,2}$	$(\mathbf{1}, 0, \mathbf{2}, -\frac{1}{2}, \mathbf{1})$
$\hat{d}^{1,2}$	$\tilde{d}_R^{1,2*}$	$d_R^{1,2*}$	$(\mathbf{1}, 0, \mathbf{1}, \frac{1}{3}, \overline{\mathbf{3}})$
$\hat{u}^{1,2}$	$\tilde{u}_R^{1,2*}$	$u_R^{1,2*}$	$(\mathbf{1}, 0, \mathbf{1}, -\frac{2}{3}, \overline{\mathbf{3}})$
$\hat{e}^{1,2}$	$\tilde{e}_R^{1,2*}$	$e_R^{1,2*}$	$(\mathbf{1}, 0, \mathbf{1}, 1, \mathbf{1})$
$\hat{H}_d$	H_d	$\tilde{H}_d$	$(\mathbf{2}, -\frac{1}{2}, \mathbf{1}, 0, \mathbf{1})$
$\hat{H}_u$	H_u	$\tilde{H}_u$	$(\mathbf{2}, \frac{1}{2}, \mathbf{1}, 0, \mathbf{1})$
$\hat{q}^3$	$\tilde{q}^3$	q^3	$(\mathbf{2}, \frac{1}{6}, \mathbf{1}, 0, \mathbf{3})$
$\hat{l}^3$	$\tilde{l}^3$	l^3	$(\mathbf{2}, -\frac{1}{2}, \mathbf{1}, 0, \mathbf{1})$
$\hat{d}^3$	$\tilde{d}_R^{3*}$	d_R^{3*}	$(\mathbf{1}, \frac{1}{3}, \mathbf{1}, 0, \overline{\mathbf{3}})$
$\hat{u}^3$	$\tilde{u}_R^{3*}$	u_R^{3*}	$(\mathbf{1}, -\frac{2}{3}, \mathbf{1}, 0, \overline{\mathbf{3}})$
$\hat{e}^3$	$\tilde{e}_R^{3*}$	e_R^{3*}	$(\mathbf{1}, 1, \mathbf{1}, 0, \mathbf{1})$
$\hat{L}$	L	ψ_L	$(\mathbf{2}, -\frac{1}{2}, \overline{\mathbf{2}}, \frac{1}{2}, \mathbf{1})$
$\hat{\tilde{L}}$	$\tilde{L}$	$\psi_{\tilde{L}}$	$(\overline{\mathbf{2}}, \frac{1}{2}, \mathbf{2}, -\frac{1}{2}, \mathbf{1})$
$\hat{K}$	K	ψ_K	$(\mathbf{1}, 0, \mathbf{1}, 0, \mathbf{1})$
$\hat{A}$	A	ψ_A	$(\mathbf{1}, 0, \mathbf{3}, 0, \mathbf{1})$

Table 3. Chiral superfields of the model MII. The first and second generation are charged under site B. The third generation are charged under site A. The representation ordering corresponds to $(SU(2)_A, U(1)_A, SU(2)_B, U(1)_B, SU(3)_c)$. The superpotential is given by Eqn. (3.3) and Eqn. (3.2). The supersymmetry breaking messenger fields are charged under site B.

Including soft breaking masses $m_L^2, m_{\tilde{L}}^2$ for the linking fields, we now expand the diagonal complex scalars into real scalar and pseudoscalar components

$$\varphi_{L1,4} = v + i\sigma_{L1,4} + \phi_{L1,4}. \tag{3.7}$$

The σ's play the role of Goldstone bosons and get eaten by the gauge fields. Minimizing the scalar potential with respect to these fields leads to the tadpole equations, which at tree-level read

$$\frac{\partial V}{\partial \phi_{L1}} = 2m_L^2 v - \frac{1}{2}vY_k\text{Re}[Y_k V^2] + v^3 Y_k^2 \tag{3.8}$$

and a similar expression for ϕ_{L4}. The value of the vev v can be obtained by requiring that the tadpoles should vanish. In practice it turns out to be much more convenient to take v as an input parameter and compute the superpotential parameter V^2 from Eqn. (3.8).

As a result of the quiver structure at different renormalisation scales Q the following occur:

- Regime 1 is characterised by $M \geq Q > v$ with the full matter content and gauge groups of the quiver.

- In Regime 2, characterised by $v > Q$, the vevs of the linking fields break the groups to the diagonal and the MSSM superfields transform under $G_{\text{Diag}} \equiv G_{\text{MSSM}}$ in the usual way.

- The $U(1)$ gauge bosons B_A, B_B mix to generate a massless and a massive state B_0 and B_m, the massless one being then the $U(1)_Y$ boson and the B_m being a heavy state. Similarly W_A^i, W_B^i mix to form the massless $SU(2)_L$ W_0^i gauge bosons as well as three heavy states W_m^i with the corresponding mixing angles discussed below. The masses of the heavy gauge bosons are simply given by

$$m_{v,i}^2 = 2(g_{A,i}^2 + g_{B,i}^2)v^2. \tag{3.9}$$

In this setup we have not considered the quiver structure for $SU(3)$. Whilst this is mostly due to practical reasons, given the difficulty of a full and proper implementation of a Higgsed $SU(3)$ as in [6, 9], it is also not necessary for our purposes. Indeed naively we sacrifice a GUT completion, but clearly we are expecting our model to be valid only up to the messenger scale in the case of GMSB and anyway it should be quite straightforward to tidy up this setup to restore gauge unification without sacrificing the key results of this work. In this sense our setup is both minimal enough, and yet concrete enough to be a "theoretical simplified model" which captures relevant features of a much larger range of possibilities, for example, it incorporates an extra $SU(2)$ and $U(1)$.

3.3 Supersymmetry breaking and soft breaking terms for gauge mediation

In principle the models above may be combined with any supersymmetry breaking scenario, for example mSUGRA, or some more phenomenological parameterisation. The model contains a large number of soft terms. The soft breaking scalar potential reads

$$
\begin{aligned}
\mathcal{V}_{soft} =\ & B_\mu \epsilon_{ij} H_u^i H_d^j + T_d^{ab} H_d^i \tilde{d}_a \tilde{q}_{bi} + T_e^{ab} H_d^i \tilde{e}_a \tilde{l}_{bi} + T_u^{ab} H_u^i \tilde{u}_a \tilde{q}_{bi} \\
& + \frac{1}{2} L_{V^2} K + T_A L_j^i A_k^j \tilde{L}_i^k + T_K K L_j^i \tilde{L}_i^j \\
& + m_{IJ}^2 \phi_I^* \phi_J + m_A^2 |A|^2 + \frac{1}{2} m_L^2 (|L|^2 + |\tilde{L}|^2) + m_K^2 |K|^2.
\end{aligned} \tag{3.10}
$$

a, b are flavour indices and i, j, k $SU(2)$ indices, which are lowered with ϵ_{ij}. The soft terms for the fermions are

$$\mathcal{L}_{soft} \supset \frac{1}{2} \left(m_{\tilde{g}} \tilde{g} \tilde{g} + m_{\tilde{B}_B} \tilde{B}_B \tilde{B}_B + m_{\tilde{W}_B} \tilde{W}_B \tilde{W}_B + m_{\tilde{B}_A} \tilde{B}_A \tilde{B}_A + m_{\tilde{W}_A} \tilde{W}_A \tilde{W}_A \right) + h.c. \tag{3.11}$$

In what follows, the RGE evolution of all parameters in this scalar potential will be accounted for at two loops.

In this work we focus on gauge mediation and take the highest scale of the RGE evolution to be M, the characteristic mass scale of supersymmetry breaking which in perturbative models is the messenger scale. As is typical of these perturbative gauge mediated supersymmetry breaking scenarios, we model the supersymmetry breaking sector with a set of messenger fields coupled to a spurion. Such a messenger sector can (and

should) be generalised [7], although we will conform to this standard paradigm. The superpotential we use is of the form

$$W_{\text{Messenger}} = X\Phi\tilde{\Phi}, \tag{3.12}$$

where X is a spurion with $X = M + \theta^2 F$ and $\Phi, \tilde{\Phi}$ are representative of fundamental and antifundamental messenger fields respectively, charged under $SU(3)_c$ and $SU(2)_B, U(1)_B$, but not under the A-site electroweak group. This leads to a scale $\Lambda = F/M$ which may differ for each gauge group so we can in general write $\Lambda_{1,2,3}$ for the three gauge groups. The messenger fields and spurion are integrated out at M to generate the soft terms, the explicit equations for which are supplied below.[2] Here we describe the gauge mediation parameterisation of the above soft terms.

3.3.1   The trilinear, bilinear and linear terms

The trilinear T-terms (or A-terms) are taken to be zero at the messenger scale, including those corresponding to Y_K and Y_A. The linear soft term L_{V^2} for the singlet ϕ_K, is also taken to be vanishing at the messenger scale. In GMSB, the bilinear term B_μ is expected to be zero at the supersymmetry breaking scale and should be generated by RG running. It is however more practical to instead solve the SM Higgs tadpole equations with respect to μ, B_μ and give $\tan\beta$ as an input. Above the scale of $G_A \times G_B$ breaking, the β-function for B_μ reads at one-loop

$$\begin{aligned}
\beta_{B\mu}^{(1)} = &\left(-\frac{3}{5}g_{A1}^2 - 3g_{A2}^2 + \text{Tr}(Y_d^\dagger Y_d) + \text{Tr}(Y_e^\dagger Y_e) + \text{Tr}(Y_u^\dagger Y_u)\right) B_\mu \\
&+ \frac{2}{5}\left(3g_{A1}^2 m_{\tilde{B}_A} + 15g_{A2}^2 m_{\tilde{W}_A} + 5\text{Tr}(Y_d^\dagger T_d) + 5\text{Tr}(Y_e^\dagger T_e) + 5\text{Tr}(Y_u^\dagger T_u)\right)\mu
\end{aligned} \tag{3.13}$$

which results in a large B_μ if the g_{Ai}'s are relatively large. The equations are similar below the quiver breaking scale. Note that there are also two-loop contributions in both regimes.

3.3.2   Gaugino soft masses

For $SU(3)_c \times SU(2)_B \times U(1)_B$ the gauginos acquire soft masses according to the standard GMSB formula

$$m_{\lambda,r} = N\Lambda\left(\frac{g_r^2}{16\pi^2}\right)g(x) \tag{3.14}$$

where $x = F/M^2$, $\Lambda = F/M$ and r refers to the corresponding gauge group. $N = (n_{5plets} + 3n_{10plets})$ is the messenger index and the function $g(x)$ is the standard function appearing in GMSB gaugino soft masses.

As the messenger sector is not charged under $U(1)_A$ and $SU(2)_A$, the corresponding gauginos are taken to be massless at the messenger scale:

$$m_{\tilde{B}_A} = m_{\tilde{W}_A} \equiv 0. \tag{3.15}$$

---

[2]It would be interesting to extend this work to include explicit messenger fields and run supersymmetrically from the GUT scale to the messenger scale, include messenger effects at the scale M and then run down to the electroweak scale.

One might imagine that such a feature could be detrimental to the low energy spectrum. However, the mass matrices of the gauginos are rather complicated including supersymmetric Dirac masses as well as the above soft terms, so this turns out not to be the case. The Majorana soft masses of the broken theory can be found by identifying the masses of the relevant components of the mixing matrices, at the threshold scale $\mathcal{O}(v)$ (see also appendix A.1). As the A-site gauginos do not obtain significant soft masses until the scale v, the RGEs of matter charged under site A will not feel these effects until a scale $Q < v$. This turns to be advantageous for naturalness as now the threshold scale $T_{scale} = v$ acts as a cutoff to the leading RGE logarithm. Such an effect will become especially important for an $SU(3)_A \times SU(3)_B$ quiver, as then the A-site gaugino would only influence the RGEs between M_{ew} and T_{scale} and have essentially no effect on the RGEs of site A matter above this scale.

3.3.3 Site A scalar soft masses

The scalar soft masses depend on the site under which the corresponding superfields are actually charged, relative to those of the messenger fields. We will always take the messenger fields to be on site B. Fields charged under G_A get soft masses at two loops from mediation along the quiver

$$m_A^2 = N \sum_{i=1,2} 2\Lambda_i^2 C_i(r) \left(\frac{g_i^2}{16\pi^2} \right)^2 s(x, y_i), \tag{3.16}$$

where $y = m_v/M$ with m_v being the heavy gauge boson mass, M the messenger scale and g_i is the corresponding coupling constant. The quadratic Casimir invariants $C_i(r)$ are $C_1(Y) = 3/5\, Y^2$ for fields charged under U(1) with hypercharge Y and $C_2(2) = 3/4$ for doublets under SU(2). In MI, where all MSSM chiral superfields reside in site A, this formula serves as a boundary condition for all electroweak contributions to the scalar soft masses. In MII, this formula only applies to the third generation sfermions and the Higgs scalars, whereas the first two generation sfermions receive their soft masses according to Eqn. (3.18).

The form of the function $s(x, y)$, associated with gauge mediation along a two site quiver, can be found in [7, 14, 15] and is given in both analytical and graphical form in appendix A.5. By inspecting figure 10 we can see how the mediation of supersymmetry breaking along the quiver has the effect of reducing the site A scalar soft masses with respect to usual gauge-mediated supersymmetry breaking. In particular, $s(x, y)$ has the limit

$$s(x, \infty) = f(x), \tag{3.17}$$

where $f(x)$ is the usual GMSB formula. This formula interpolates between $y \to \infty$ of GMSB and the suppressed scalar regime as $y \to 0$, where scalars get their leading soft mass at three loops from additional contributions, which arise anyway from RG evolution.

3.3.4 Site B scalar soft masses

Scalar fields charged under G_B and $SU(3)_c$ receive standard GMSB soft masses according to

$$m_B^2 = N \sum_{i=1,2,3} 2\Lambda_i^2 C_i(r) \left(\frac{g_{Bi}^2}{16\pi^2} \right)^2 f(x). \tag{3.18}$$

The quadratic Casimir invariants are $C_1(Y_B) = 3/5 Y_B^2$ for fields with charge Y_B under $U(1)_B$ whereas $C_2(2) = 3/4$ for the linking fields L and $C_2(3) = 2$ for the $SU(2)_B$ adjoint A field. All coloured scalars in our setup are $SU(3)$ triplets, for which $C_3(3) = 4/3$. Note that in the case of site A coloured scalars, the full soft mass is given by the sum of Eqn. (3.16) and the third term of Eqn. (3.18).

3.3.5 The singlet scalar K soft mass

The superfield K is a gauge singlet and its scalar soft mass is vanishing at the messenger scale,

$$m_K^2 = 0. \tag{3.19}$$

It evolves a positive value through Eqn. (A.29) and so does not pose a phenomenological issue, but if one did wish to assign a tree level soft mass, two approaches are possible: it may be interesting to consider that it is not a singlet under some other group or that it couples directly to messenger fields through a term of the form $K\Phi\tilde{\Phi}$. In this later case it can develop a one-loop soft mass.

3.3.6 Linking scalar soft masses

The linking fields formally get their soft masses from applying Eqn. (3.18) to describe the soft terms for m_L^2 and $m_{\tilde{L}}^2$. We will however not be using this formula in order to compute the linking field soft masses. Instead, we will promote them to free parameters of the model. The reasons for this choice will be clarified in the following section. To be noted is that in this setup the two linking field masses are equal, $m_L^2 = m_{\tilde{L}}^2$.

3.4 Linking to the MSSM

Below the quiver breaking scale the gauge group and particle content of the model are those of the minimal supersymmetric standard model with gauge groups $SU(3)_c \times SU(2)_L \times U(1)_Y$. The gauge couplings between the unbroken and the broken theory are matched as

$$\frac{1}{g_i^2} = \frac{1}{g_{Ai}^2} + \frac{1}{g_{Bi}^2} \iff g_i^2 = \frac{g_{Ai}^2 g_{Bi}^2}{g_{Ai}^2 + g_{Bi}^2} \ , \tag{3.20}$$

with $i = 1, 2$ for $U(1)_Y \times SU(2)_L$. If one of the two gauge couplings is strong, the other should be weak. Then at low energies the diagonal or MSSM gauge coupling will be of the order of whichever is weaker. This is a key feature which allows for these models to lift the

tree-level Higgs mass whilst being consistent with perturbative unification. The various gauge couplings of the model are simply related through two rotation angles [3]

$$\cos \theta_i = \frac{g_i}{g_{Ai}}, \quad \sin \theta_i = \frac{g_i}{g_{Bi}}. \tag{3.21}$$

In appendix A.4 we present additional comments on threshold effects that enter the coupling constants and other parameters calculation below the quiver breaking scale. The angles θ_1, θ_2 are free parameters of our setup. Varying these amounts to changing the relative strengths between each site and we typically choose the A-sites to be stronger to enhance additional contributions to the Higgs mass, as we will explain below.

One of the most interesting features of this class of models is that non-decoupled D-terms may arise [3, 16] in the low energy Lagrangian. The real uneaten scalar components of the linking fields appear in both the A and B site scalar D-term potential and when integrated out generate an effective action which includes the terms

$$\delta \mathcal{L} = -\frac{g_1^2 \Delta_1}{8} (H_u^\dagger H_u - H_d^\dagger H_d)^2 - \frac{g_2^2 \Delta_2}{8} \sum_a (H_u^\dagger \sigma^a H_u + H_d^\dagger \sigma^a H_d)^2, \tag{3.22}$$

where

$$\Delta_1 = \left(\frac{g_{A1}^2}{g_{B1}^2} \right) \frac{m_L^2}{m_{v1}^2 + m_L^2} \quad , \quad \Delta_2 = \left(\frac{g_{A2}^2}{g_{B2}^2} \right) \frac{m_L^2}{m_{v2}^2 + m_L^2}. \tag{3.23}$$

It is particularly informative to see how in this class of models, these terms can work to lift the Higgs mass without large radiative corrections. In the MSSM, the one-loop Higgs mass in the limit $m_{A^0} \gg m_Z$ can be written as [17]

$$m_{h,1}^2 \simeq m_z^2 \cos 2\beta + \frac{3}{4\pi^2} \frac{m_t^4}{v_{ew}^2} \left[\ln \frac{M_S^2}{m_t^2} + \frac{X_t^2}{M_S^2} \left(1 - \frac{X_t^2}{12 M_S^2} \right) \right] \tag{3.24}$$

where $M_S^2 = m_{\tilde{t}_1} m_{\tilde{t}_2}$ for $m_{\tilde{t}_1}$, $m_{\tilde{t}_2}$ as defined in appendix A.1, and v_{ew} is the electroweak Higgs vev, such that the upper limit on the tree level Higgs mass $(m_{h,0})$ is set by the Z boson mass m_z. This expression assumes that the left and right-handed soft masses of the stops are equal. Note that $X_t = A_t - \mu \cot \beta$, and for convenience the sfermion mixing matrices are provided explicitly in Eqn. (A.12) of appendix A.2. In our case however, there may in principle be a sizeable shift to the Higgs mass at tree level $m_{h,0}$, which takes the precise form,

$$m_{h,0}^2 = \left[m_z^2 + \left(\frac{g_1^2 \Delta_1 + g_2^2 \Delta_2}{2} \right) v_{ew}^2 \right] \cos 2\beta. \tag{3.25}$$

Arguably this enhancement is favoured over that of the NMSSM for a simple reason: in the NMSSM typically

$$m_{h,0}^2 = m_z^2 \cos 2\beta + \lambda^2 v_{ew}^2 \sin 2\beta \tag{3.26}$$

---

[3]Here we should stress an important notation subtlety. In all relations applying to the messenger scale as well as in all RGE expressions, the $U(1)$ coupling constants are taken to be $SU(5)$ GUT-normalized, so for example $g_1 = g_{1,GUT} = \sqrt{5/3} g'$, with g' being the usual Standard Model hypercharge coupling constant. In all other relations, the GUT normalization is dropped and g_1 identical to g'. This is done in order to follow the SARAH package conventions.

where λ is the coupling between the Higgs singlet and doublet fields appearing in the superpotential term $\lambda S H_u H_d$. This creates a tension between wanting a large $\tan\beta$ to enhance the first term, but a small $\tan\beta$ for the second, forcing one to accept very large values of λ. As a result λ ends up non perturbative before the GUT scale.

It is the above observation that forms the basis for the construction of natural spectra in the class of models that we examine: the Higgs mass can now be substantially increased already at tree-level when these new contributions become large. Of course this enhancement is completely independent of the method by which supersymmetry breaking effects are transmitted to the MSSM. We have simply chosen GMSB in this paper on the one hand to demonstrate that it is still a natural candidate for supersymmetry breaking mediation, and on the other hand because in our electroweak GMSB quiver the sleptons can be naturally lighter than their coloured counterparts. This potential enhancement of the tree level Higgs mass is only significant in certains areas of the model's full parameter space. Concretely, for this contribution to be sizeable we must have $g_{Ai}^2/g_{Bi}^2 \geq 1$ and $m_L \sim \mathcal{O}(m_{v,i})$.

However, this mechanism introduces some additional fine-tuning to the theory, since the Higgs mass now receives an additional quadratically divergent contribution at one loop, induced by the linking fields and cut off by m_L^2. This additional fine-tuning should be kept under control in order to not counterbalance the improved naturalness of the model with respect to traditional mGMSB. An estimate of the maximal size of m_L can be found following the arguments of [4]: demanding less than 10% additional fine tuning approximately bounds

$$\frac{g_{SM}^2 \Delta}{16\pi^2} \frac{m_L^2}{m_h^2} < 10. \tag{3.27}$$

Requiring, for example, $\Delta = 0.2$ in Eqn. (3.23) allows m_L^2 in the $10^6 - 10^8 \text{GeV}^2$ range and sets an upper value $v < 10^5$ GeV so that the additional D-terms do not decouple. So in summary we would ideally want $v < 10^5$ GeV and $m_L < 10$ TeV. Note that v is also bounded from below both by electroweak precision tests and direct searches for new gauge bosons.

The non-decoupled D terms also appear in the tadpole equations

$$\frac{\partial V}{\partial \phi_d} = \frac{1}{8}\Big(- 8v_u \text{Re}[B_\mu] + (g_1^2 + g_2^2 + g_1^2\Delta_1^2 + g_2^2\Delta_2^2)v_d^3 \tag{3.28}$$
$$+ v_d[8m_{H_d}^2 + 8|\mu|^2 - (g_1^2 + g_2^2 + g_1^2\Delta_1^2 + g_2^2\Delta_2^2)v_u^2]\Big)$$

$$\frac{\partial V}{\partial \phi_u} = \frac{1}{8}\Big(- 8v_d \text{Re}[B_\mu] + 8v_u|\mu|^2 \tag{3.29}$$
$$+ v_u[8m_{H_u}^2 - (g_1^2 + g_2^2 + g_1^2\Delta_1^2 + g_2^2\Delta_2^2)(-v_u^2 + v_d^2)]\Big)$$

modifying the vacuum structure, as well as the Higgs mixing matrices, which may be found in appendix A.2.

Additional soft mass terms for all scalars appear in regime 2 of the model at effective one loop, from integrating out the heavy gauge and linking fields [6]

$$\delta m_{\tilde{f}}^2 = \sum_i \left(\frac{g_i}{4\pi}\right)^2 C_k^{\tilde{f}} \left[m_{v_i}^2 \tan^2\theta_i \log\left(1 + \frac{2m_L^2}{m_{v_i}^2}\right) + 2\sin^2\theta_i(1 - 3\sin^2\theta_i)m_{i,B}^2\right] \quad (3.30)$$

which are also implemented into the model and importantly the soft mass parameters are matched across the threshold scale.[4]

3.5 An extra dimensional digression

Quiver models are naturally related to extra dimensional setups through deconstruction [7, 15]. It should therefore be expected that these non decoupled D-terms, Eqn. (3.23), have a natural interpretation in terms of extra dimensional models. We swiftly sketch and motivate this relationship which certainly warrants further study on its own. The quiver construction may be related to $\mathcal{N} = 1$ super Yang-Mills (or $\mathcal{N} = 2$ [18–20]) in five dimensions [12], which contains a vector multiplet and chiral adjoint $V + \Phi$. Suppose we compactify on four flat dimensions times a small interval of length R. The scalar component of $\Phi = (\Sigma + iA_5)$ and in analogy to the quiver, A_5 plays the role of the Goldstone bosons and are eaten to generate the Kaluza-Klein masses such that we may identify $1/R \sim v$ of Eqn. (3.7). To obtain the non decoupled D-terms we write the lagrangian in the off-shell formulation

$$\mathcal{L}_5 = \frac{1}{2}D^2 + D(\partial_5\Sigma) - \frac{1}{2}\partial_\mu\Phi\partial^\mu\Phi^* + m_{\text{soft}}^2\Sigma\Sigma + ... \quad (3.31)$$

The ellipses denote not just the rest of the bulk action but also any terms generated on bulks and boundaries that may be of use such as the boundary terms

$$\int_{\partial\mathcal{M}} (\Sigma D + ...). \quad (3.32)$$

To see how this action may generate a non decoupled D-term we define $\mathcal{H} = (H_u^\dagger H_u - H_d^\dagger H_d)$. Then, there may be bulk or boundary terms of the usual form

$$\mathcal{L} \supset \frac{1}{2}\mathcal{H}D. \quad (3.33)$$

Integrating out the auxiliary scalar field D gives rise to the D-term scalar potential. The field Σ, the real uneaten scalar degrees of freedom, corresponds to the real uneaten degrees of freedom in the linking fields $L, \tilde{L}$ of the quiver. It is this field Σ, when integrated out which generates the non decoupled D-term Eqn. (3.23). In such a scenario, the m_v of the quiver is related to the Kaluza-Klein mass scale m_{kk} which is $O(1/R)$, the effective length scale of the extra dimension. As such, for these terms to be of relevance $\pi/R \leq m_{\text{soft}}$. We hope to return to this topic in a further publication, but for now we effectively model this feature with quiver models as they are a more controlled environment which are more amenable to spectrum generators. It is certainly interesting to speculate that as our model has a v of $\mathcal{O}(10^4)$ GeV, that this corresponds to an "effective" extra dimensional length scale of roughly $\mathcal{O}(10^{-18})$ cm.

---

[4]There are further three loop terms if the $SU(3)$ sector is quivered.

4 Tools and Observables

In order to study the low-energy phenomenology of our setup in a consistent manner, it is necessary to perform the RGE evolution of all couplings and mass parameters from the highest energy scale of the theory down to the TeV scale, properly imposing all boundary conditions. Here we describe the construction of a tailor-made spectrum generator for the quiver model. We further discuss the parameter space we adopt as well as the constraints it is subject to.

4.1 Implementing a quiver framework for phenomenological studies

In order to perform the RGE evolution of the models' parameters and masses and compute the resulting low-energy particle spectra, we implemented the two model variants into the publicly available Mathematica package SARAH 3.3 [21–23]. SARAH is a "spectrum generator generator", which includes a library of models that may communicate with HEP tools that are widely used in most phenomenological studies [24–35]. In particular, SARAH performs the task of generating Fortran routines compatible with the SPheno spectrum generator [22].

In order to implement our model, we have used the possiblity offered by the package to implement and link two different "regimes". These regimes correspond to those introduced in section 3.2, each being characterised by a set of gauge groups, a particle content and a superpotential that need to be specified. Regime 1 includes, for both models MI and MII, the full $G_A \times G_B \times SU(3)_c$ gauge group along with the full quiver particle content, while the superpotential is given by Eqns.(3.1) and (3.2) for MI and by Eqns.(3.3) and (3.2) for MII. In both cases in regime 2 we have the MSSM, which we supplement by hand by an effective action to account for and study the effects of the non-decoupled D-terms, which are of crucial importance, as discussed in section 3.4. We would have preferred to implement our model using a single regime such that these terms would be automatically generated, and as there are other terms for other fields, however we found it was not practical to integrate out so many fields in full. Moreover it was preferable to include an additional regime with the MSSM gauge and matter configuration to ease communication of SPheno with packages such as HiggsBounds, used to check the compatibility of the model with experimental constraints as discussed below.

In addition to these ingredients, we need to specify on the one hand boundary conditions for all soft parameters at the messenger scale M and on the other hand matching conditions for the parameters of the two regimes at the $G_A \times G_B$ breaking scale which we typically take to coincide with v, the linking field vev. The boundary conditions are applied according to the discussion and relations given in section 3.3, while the matching conditions follow the lines described in section 3.4.

The renormalization group equations for both regimes are then calculated by SARAH at two loops and appropriate Fortran routines are generated that can then be taken over by SPheno to perform the numerical analysis. Concretely, the implementation includes full one- and two- loop RGEs for five gauge groups, mixing matrices for all fields in the quiver and the MSSM including associating goldstones with massive gauge bosons and gauge fix-

ings, full two-loop RGEs for the vev of the linking fields themselves, two-loop RGEs for $B\mu$, loop-level solutions for the tadpole equations, one- and two- loop anomalous dimensions for all fields and two-loop RGEs for all soft breaking parameters, linear, bilinear and trilinear. The MSSM particle masses are computed at one loop, however the full two-loop corrections to the Higgs mass are implemented in `SPheno` following the calculation in Refs. [36–39].

All in all, the RGE evolution is described by three energy scales

$$M_{\text{messenger}} \longrightarrow T_{\text{scale}} \longrightarrow M_{ew}.$$

Following standard practice, the highest energy scale of the theory is taken to be the messenger scale M, where all boundary conditions resulting from the quiver structure, including exact formulae for GMSB soft masses have been implemented and imposed. Again as usual, the running ends at the electroweak scale, which is used as an input scale for the MSSM parameters. The intermediate mass scale T_{scale} is associated with the quiver breaking scale as it separates the two regimes, and at this scale appropriate matching boundary conditions are applied including finite shifts that result from integrating out the heavy fields of the theory (see appendix A.4). We choose it to be equal to the vev of the linking fields, $T_{\text{scale}} = v$. All soft terms of regime 2 are matched to regime 1 as described in section 3.4 and for the soft masses of the winos and binos in appendix A.1. Note that the gluino finite shifts are also accounted for as given in appendix A.4.

It is important to stress that the high-scale boundary conditions themselves may be seen as being separable from the model (the matter content, gauge groups and superpotential) and may be changed with ease, if one wished to explore, for example, different supersymmetry breaking scenarios.

The implementation detailed above, i.e. the construction of a tailor-made spectrum generator for our model, allows us to create a model file for `SPheno`, which further permits us to study a quiver model in a complete manner, as we can study the influence of RG effects of all the gauge groups and matter content in the highest regime to the low energy spectrum, at the two-loop order. On the practical level, this model can also serve as a first step for the implementation of more complete or complicated setups, such as a model including an additional $SU(3)$. It would further be trivial to change the representation assignments of the Higgs fields in order to study chiral non-decoupled D-terms [40] or flavour models, with the same precision. However, we point out that the implementation of the electroweak only quiver studied here leads to an interesting phenomenology in its own right, allowing for naturally (although moderately) heavier squarks relative to sleptons.

4.2 Parameter space and constraints

It is now useful to describe the process through which we choose our parameter space and the regions we will study in the next section. We moreover describe some preliminary findings that could be of interest for model-building purposes.

4.2.1 Choosing the parameter space

The electroweak quiver we consider can be described by a basic set of six parameters

$$M, \Lambda, v, \tan\beta, \theta_1, \theta_2, \tag{4.1}$$

where M is the messenger scale, the SUSY breaking scale $\Lambda = F/M$, F being the SUSY breaking F-term, $\tan\beta$ is the Higgs vev ratio and θ_1, θ_2 are the mixing angles between sites A and B for $U(1)$ and $SU(2)$ respectively.

As an initial step, we performed extended scans over large regions of parameter space for MI, imposing the full set of GMSB boundary conditions described in section 3.3, including the exact relations Eqn. (3.18) for the linking field soft masses. We focused in particular on regions where $v \lesssim 40$ TeV, where according to the discussion of section 3.4 the non-decoupled D-terms should be most efficient in lifting the tree-level Higgs boson mass. A first finding of these searches is that we could not find viable points when the linking field vev was much below 10 TeV, as often here either the A-site couplings become non-perturbative before the messenger scale, the electroweak vacuum becomes unstable or the RGE code simply wouldn't converge for the numerical precision requirements imposed (a relative error of 0.5%). Where none of these issues occur, the values of Λ are typically low and close to v, such that the linking fields soft masses m_L are too low for the D-terms to have an important impact on the Higgs mass.

Motivated by the perturbativity issues, we implemented MII where we expect that by removing some of the matter fields from site A the RGE running will be reduced [9]. We found that although the situation does improve, it still seems to be quite difficult to achieve substantial contributions to the Higgs tree-level mass from the non-decoupled D-terms due to the fact that m_L^2 is again driven too low.

These results lead us to slightly enlarge our parameter space by promoting the linking field squared soft mass m_L^2 to be a free parameter instead of being given by Eqn. (3.18). This is interesting from a theoretical perspective, as it motivates pursuing models that might provide the additional contribution to m_L^2 needed in order to achieve a substantial D-term contribution to the Higgs mass. For example, it would be interesting to study whether this can be realized in extensions to the model including an additional $SU(3)$ or $U(1)$ kinetic mixing. Within the scope of our work, the choice to make m_L^2 free can be seen as a phenomenological parametrization of the linking field soft masses along the lines of similar choices made in many supersymmetry breaking mediation schemes.

With this small modification, we find that it is indeed perfectly possible to achieve the required D-term size in order to reproduce the observed Higgs mass while keeping the stop masses well below 2 TeV. Furthermore as expected, the mediation of SUSY breaking along the quiver acts as a suppression mechanism for the uncoloured sparticle masses, yielding electroweakinos and sleptons lying roughly in the range [400, 1000] GeV, which is on the boundary of being within the LHC reach [41, 42]. At this point, due to the differing bounds on coloured and non-coloured sparticles at the LHC, we introduce a second modification to the original setup that consists of dissociating the scale Λ_3 from $\Lambda_{1,2}$. Note however that this is a minor modification as the two scales will not differ by orders of magnitude but only

by $\mathcal{O}(1)$ multiplicative factors. We will see that this setup allows for a rich phenomenology with interesting features.

4.2.2 Constraints

We carried out extensive scans of the parameter space described in the previous paragraph within generous intervals. We are interested in areas of parameter space which are characterised by low values of v and moderate splittings between v and m_L, such that the additional D-terms do not decouple from the low-energy theory and the uncoloured scalars are light. In what follows, we will therefore present results that concern a subregion of the parameter space that meets a series of requirements.

First, we wish to obtain a Higgs mass lying in the range $[122.5, 128.5]$ GeV. This interval envelops on the one hand the experimental uncertainty in the Higgs mass measurement [1, 2, 43], while being sufficiently generous to account for uncertainties in the theoretical mass spectrum determination [44, 45][5]. For naturalness reasons, we require this value for the Higgs mass to be achieved for stop masses as low as possible. The stop mass is governed by Λ_3, which also controls the masses of the lower generation squarks and the gluino. Strong exclusions on these masses arise from ATLAS and CMS null searches for jets plus missing energy, e.g. $m_{\tilde{g}} > 1600$ GeV for $m_{\tilde{q}_{1,2}} > 2000$ GeV [47, 48]. We are guided by these bounds in choosing a lower limit for Λ_3. Note that in this work, we choose not to quantify the amount of fine-tuning for each point of the models we study, which constitutes a work in its own right involving numerous subtleties (see for example the recent discussion in [49]). It is however at least clear that qualitively, having stops lighter than benchmark minimal GMSB improves the relative naturalness of the model, and this motivates our choice of upper limit on Λ_3.

At the same time, according to the comments made in section 3.4, we should avoid reintroducing excessive fine-tuning via the non-decoupled D-terms. Moreover, in order for the setup to be realistic, we must satisfy the condition $m_L^2 < m_v^2$, but not approach the limit $m_L^2 \ll m_v^2$ where the quiver-induced D-terms decouple. These requirements lead us to choose m_L^2 within the range $[10^7, 10^8]$ GeV^2. Also note that as mentioned above, for very low values of v SPheno faces convergence issues, and in any case such low values would be in conflict with searches for new gauge bosons at the LHC. The parameter $\Lambda_{1,2}$ is mainly subject to constraints from searches for charged sleptons and charginos at LEP, i.e. 92 GeV for charginos degenerate with the lightest neutralino, and 103.5 GeV otherwise [50]. Lower limits on sleptons staus and sneutrinos of 68 and 51 GeV respectively were also obtained at LEP [51–53]. Finally, given that the non-decoupled D-terms contribute a shift to the Higgs mass as m_Z does, i.e. with a factor $\cos 2\beta$ (Eqn. (3.25)), as opposed to the factor $\sin 2\beta$ in the NMSSM (Eqn. (3.26)), we explore a rather standard MSSM-like range for $\tan\beta$.

From our numerical analysis we find that this set of requirements is satisfied by adopting the following parameter value ranges

$$2.1 \times 10^5 \text{ GeV} \leq M \leq 3.0 \times 10^5 \text{ GeV} \tag{4.2}$$

---

[5]Throughout our calculations we assume a constant moderate top quark mass of $m_t = 173$ GeV [46].

Observable	Accepted range
$B_s \to X_s \gamma$	$[2.78, 4.32] \times 10^{-4}$ [55]
δa_μ	$< 20 \times 10^{-10}$ [46]
$\Delta \rho$	$< 1.2 \times 10^{-3}$ [46]
$BR(B_s \to \mu^+\mu^-)$	$< 7.7 \times 10^{-9}$ [56]

Table 4. Low-energy observable constraints imposed in our analysis.

$$4.0 \times 10^4 \text{ GeV} \leq \Lambda_{1,2} \leq 1.9 \times 10^5 \text{ GeV}$$

$$1.9 \times 10^5 \text{ GeV} \leq \Lambda_3 \leq 2.1 \times 10^5 \text{ GeV}$$

$$1 \times 10^7 \text{ GeV}^2 \leq m_L^2 \leq 1 \times 10^8 \text{ GeV}^2$$

$$1.5 \times 10^4 \text{ GeV} \leq v \leq 4 \times 10^4 \text{ GeV}$$

$$5 \leq \tan\beta \leq 30$$

$$0.8 \leq \theta_1, \theta_2 \leq 1.4$$

We have moreover chosen sign$\mu = +1$, a low value for the messenger index, $N = 1$, and a fixed common value for the A and K field Yukawa couplings $Y_A = Y_K = 0.8$.

Apart from the theoretical and experimental constraints so far mentioned, the low-energy spectrum is subject to further bounds. In the Higgs sector, in addition to obtaining the lightest Higgs boson mass within the observed region, we must ensure that its properties and decay modes comply to current LHC observations. As an example, it is known that enhancing the Higgs mass through non-decoupled D-terms enhances simultaneously the Higgs boson couplings to down-type quarks [4, 10, 40]. In order to test whether the Higgs sector is compatible with the constraints coming from the LHC and the TeVatron, we have linked `SPheno` to `HiggsBounds-4.0.0` [32]. Taking our analysis a step further, we have also linked `SPheno` to `HiggsSignals-1.0.0` [54], which allows us to test in particular whether the lightest Higgs boson properties are in agreement with all relevant existing mass and signal strength measurements from the LHC and TeVatron.

Finally, we use the in-built functionalities of `SPheno` in order to apply a set of necessary low-energy constraints, all of which are taken at 3σ: the SUSY contributions to the muon anomalous magnetic moment δa_μ and the branching ratios $BR(B_s \to X_s \gamma)$ and $BR(B_s \to \mu^+\mu^-)$ and, due to the presence of relatively light sfermions in our spectra, the ρ parameter. The allowed ranges used for these observables are shown in table 4, where theoretical uncertainties and experimental errors are added in quadrature.

5   Results

Having described our model, and how it is implemented in `SARAH`, we turn to study the low scale spectrum, which we find has several interesting features. Examples of complementary representative points, one for MI and two for MII, are given in table 5.

	MI	MIIa	MIIb
Input values			
M	233 TeV	288 TeV	260 TeV
$\Lambda_{1,2}$	44.9 TeV	85.6 TeV	111 TeV
Λ_3	190 TeV	206 TeV	208 TeV
m_L^2	47.3 TeV^2	83.3 TeV^2	86.2 TeV^2
v	26.2 TeV	26.5 TeV	25.4 TeV
θ_1, θ_2	1.18, 1.13	1.09, 1.33	1.05, 1.04
$\tan\beta$	16	12	28
Squark sector			
$m_{\tilde{t}_1}$	1.84 TeV	1.99 TeV	409 GeV
$m_{\tilde{t}_2}$	1.98 TeV	2.06 TeV	3.49 TeV
A_t	-442 GeV	-146 GeV	-141 GeV
$m_{\tilde{b}_R}$	1.95 TeV	2.05 TeV	2.56 TeV
$m_{\tilde{q}_{12,L}}$	2.05 TeV	2.12 TeV	2.19 TeV
$m_{\tilde{q}_{12,R}}$	1.97 TeV	2.10 TeV	2.14 TeV
Slepton sector			
$m_{\tilde{l}_{12,L}}$	738 GeV	314 GeV	515 GeV
$m_{\tilde{l}_{3,L}}$	736 GeV	315 GeV	440 GeV
$m_{\tilde{l}_{12,R}}$	901 GeV	183 GeV	262 GeV
$m_{\tilde{l}_{3,R}}$	899 GeV	110 GeV	4.31 TeV
Gaugino sector			
$m_{\tilde{\chi}_1^0}$	53.2 GeV	116 GeV	154 GeV
$m_{\tilde{\chi}_2^0}$	99.3 GeV	242 GeV	306 GeV
$m_{\tilde{\chi}_3^0}$	187 GeV	750 GeV	818 GeV
$m_{\tilde{\chi}_3^0}$	222 GeV	755 GeV	823 GeV
$m_{\tilde{\chi}_1^\pm}$	96.8 GeV	242 GeV	306 GeV
$m_{\tilde{\chi}_2^\pm}$	225 GeV	756 GeV	823 GeV
$m_{\tilde{g}}$	1.62 TeV	1.66 TeV	1.75 TeV
Higgs sector			
m_{h_0}	125 GeV	127 GeV	125 GeV
m_{H_0}	720 GeV	792 GeV	885 GeV
m_{A_0}	721 GeV	796 GeV	894 GeV
$m_{H_\pm}$	726 GeV	799 GeV	893 GeV

Table 5. Mass spectra of three example points for MI and MII, along with the associated input parameters as defined in section 4.2. Note that $m_{\tilde{f}_{12,L/R}}$ and $m_{\tilde{f}_{12,L/R}}$ are the masses of the lower and third generation left/right-handed squarks and sleptons, and that the sneutrino and sbottom masses can be inferred via $m_{\tilde{\nu}_i} \sim m_{\tilde{f}_{i,L}}$, $m_{\tilde{b}_L} \sim m_{\tilde{t}_L}$.

In table 5 we observe that particles of the electroweak sector can be substantially lighter than those of the coloured sector. This arises due to the quiver structure of the model, as explained in section 3.3, which provides a suppression factor $s(x, y)$ for the non-coloured scalar masses, for details see appendix A.5. The suppression is further enhanced by the fact that we have chosen to study the range of parameter space where $\Lambda_{1,2} < \Lambda_3$. Therefore it is possible for the masses of electroweakinos, sleptons and the heavy Higgs bosons to lie well below 1 TeV. One observes in table 5 that this results in the next-to-lightest supersymmetric particles (NLSPs), being either a neutralino, as in MI and MIIb, or stau, as in MIIa. A sneutrino NLSP is also possible as will be discussed in detail later in this section. As we only consider a single $SU(3)$ gauge group at the high scale, the masses of the coloured sparticles do not experience this suppression. This means that the coloured sector lies in general between 1.5 and 2.5 TeV, the stops being the lightest squarks. However, in MII, a splitting is generated between the left and right stop soft masses, for reasons discussed below, as shown in point MIIb of table 5. In the following we will study the spectra of these models in terms of their compatibility with the current experimental constraints described in the previous section and the prospects for detecting signs of TeV-scale sparticles in the near future.

5.1 The Higgs mass and couplings

As the non-decoupled D-terms lift the tree-level Higgs mass, as in Eqn. (3.25), here we investigate the range of stop masses in these models for which m_h lies in the desired range, and how the stop contribution compares to that of the non-decoupled D-terms. The same non-decoupled D-terms can affect the couplings of the Higgs, so we further investigate these couplings in light of current and future experimental measurements.

5.1.1 The Higgs mass

As mentioned in section 4.2, we have chosen Λ_3 such that the masses of gluino and the first and second generation squarks lie above the LHC exclusion limits. In MI, this translates into the stop masses being close to 2 TeV, which means that the shift in the tree-level Higgs mass required in order to obtain $m_h \sim 125.5$ GeV is small, and the required soft mass of the linking field remains below 10 TeV. The situation is fairly similar in MII, however we find that there is a slight tendency for a splitting to arise between the left and right-handed stop soft masses, due to the RGEs driving the left-handed mass downwards, and the right-handed mass upwards. This can be understood in terms of the differences between the RGE equations for the two models, where in MII above the quiver-breaking scale the Higgs soft masses are only affected by the third generation squarks, whereas for MI the Higgs soft mass RGE equations contain all generations. This results in a larger splitting between the up and down type Higgs soft masses which further generates a larger splitting between the left and right handed stop. The distribution of the masses of the light and heavy stops i.e. $m_{\tilde{t}_1}$ and $m_{\tilde{t}_2}$ as defined in appendix A.1 for the two models are displayed in figure 3. Here the allowed points are shown in yellow and those points excluded by the various constraints described in section 4.2 in grey. We clearly observe that for MII
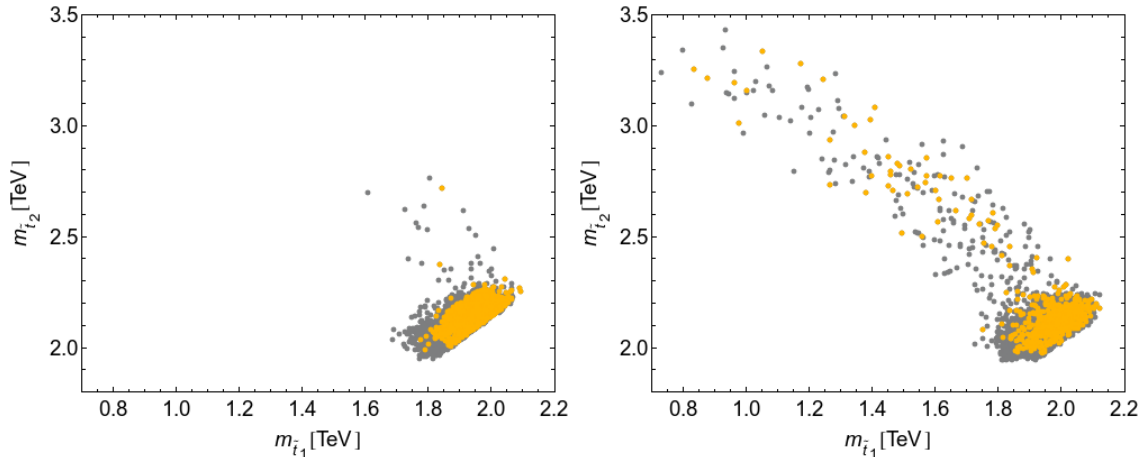
Figure 3. The mass of the heavy stop $m_{\tilde{t}_2}$ as a function of $m_{\tilde{t}_1}$ for MI (left) and MII (right). Points satisfying low-energy and the Higgs mass constraints are shown in yellow, whereas the remaining excluded points are shown in grey.

a larger splitting between the stops is possible, and the lighter stop may be as light as 400 GeV, as seen in the benchmark point MIIa in table 5.

In figure 4 we have plotted the Higgs mass as a function of $\tan\beta$ for the two variants of our model. Here the bright red points respect $m_{\tilde{t}_1} < 2$ TeV and all constraints imposed, the pale red points only comply with the low-energy constraints and the grey points are excluded. The full two-loop corrections to the Higgs mass are implemented in SPheno following the calculation in Refs. [36–39]. We conclude that a Higgs mass within the limits $\sim 125.5 \pm 3.0$ GeV is achievable in both MI and MII. Note that the larger range in m_h for MII can be explained by the larger range in stop masses. Indeed, when the left and right handed stop soft masses are not equal, as shown in figure 3 for MII, the simplified expression for the one-loop Higgs mass given in Eqn. (3.24) is no longer valid. An additional correction must be added to Eqn. (3.24) of the form [57]

$$\Delta m_{h,1}^2 = \frac{3m_Z^2}{16\pi^2 v_{ew}^2}(1 - \frac{8}{3}\sin\theta_W^2)\cos 2\beta \, m_t^2 \ln\left(\frac{m_{\tilde{q}_L^3}^2}{m_{\tilde{u}_R^3}^2}\right), \qquad (5.1)$$

which for the case $m_{\tilde{q}_L^3}^2 < m_{\tilde{u}_R^3}^2$ in MII induces an enhancement to the Higgs mass of around 1-2 GeV. Note that the sfermion mixing matrix is defined in appendix A.2. As the bright red points correspond to $m_{\tilde{t}_1} < 2$ TeV, this further demonstrates that the effect of the non-decoupled D-term seems to reduce the fine tuning by allowing lighter stops than in standard GMSB.

To make the distinction between the non-decoupled D-term and radiative, i.e. stop sector, contributions to the Higgs mass clearer, we compare the tree-level result $m_{h,0}$ to the full two-loop result $m_{h,2}$ in figure 5. Here the bright blue points respect $m_{\tilde{t}_1} < 2$ TeV and all constraints imposed, the pale blue points only satisfy low-energy restrictions and the grey points are excluded. As opposed to the mGMSB result, where $m_{h,0}$ is bounded by m_Z,
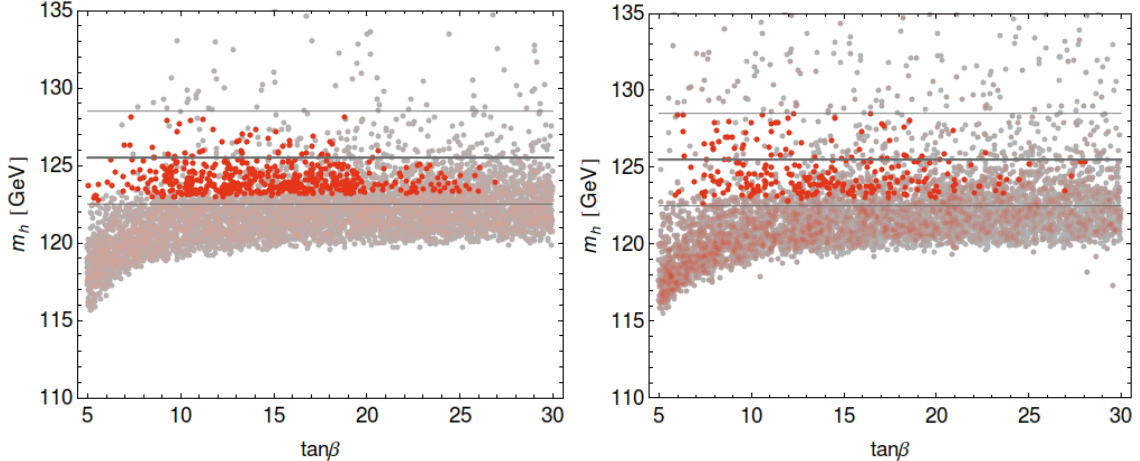
Figure 4. The Higgs mass as a function of $\tan\beta$ for MI (left) and MII (right). Points satisfying all constraints and $m_{\tilde{t}_1} < 2$ TeV are bright red, whereas paler points indicate that stop masses are in the range $2\,\text{TeV} < m_{\tilde{t}_1} < 2.3$ TeV and only low-energy constraints are satisfied. Grey points are excluded. The thick (thin) grey lines denote the central value (uncertainty) on m_h.

here we observe that a shift of up to 10 GeV is possible for both MI and MII, while keeping $m_L < 10$ TeV. This in turn means that the contribution of the radiative corrections required to achieve $m_h \sim 125.5$ GeV is diminished, rendering the model more natural. Interestingly, the splitting of the stops observed in MII results in a distinct difference between the two plots in figure 5, which can be understood from Eqn. (5.1). Despite the fact that the range in Λ_3 is the same for both MI and MII, the stop splitting enhances the size of the radiative corrections, resulting in a smaller shift in the tree level Higgs mass required to obtain a value of m_h in agreement with experiment.

5.1.2 The Higgs couplings

Since the discovery of the Higgs boson, not only has its mass been used to discriminate between supersymmetric models but also its couplings, see e.g. [4, 58, 59]. The deviation of these couplings from the SM can be parameterised via the set of ratios r_i, for $i = b, \gamma, g$ etc, where

$$r_i = \frac{\Gamma_{\text{MSSM}}(h \to ii)}{\Gamma_{\text{SM}}(h \to ii)}. \tag{5.2}$$

The r_i are further related to the signal strengths μ_i normally quoted by ATLAS and CMS, see e.g. Refs. [60, 61]. Note that the errors on the measured signal strengths are still too large to make detailed interpretations about the potential underlying SUSY model, and at present the μ_i are all SM compatible, and therefore we will not tackle a precise calculation of the various signal strengths in this work. As mentioned, we however make sure that the lightest Higgs boson signal strengths are in agreement with the existing LHC and TeVatron measurements within 3σ, employing the `HiggsSignals` code. Recent studies by both ATLAS and CMS [41, 42] have found that with a luminosity of 300 fb^{-1} at the 14 TeV LHC, an uncertainty on the measurement of r_b should only be 10–13%. A
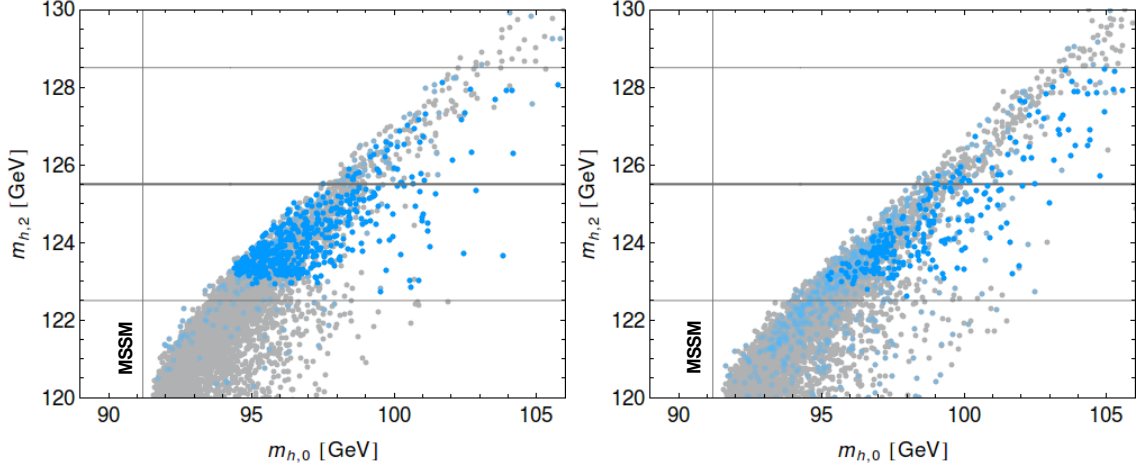
Figure 5. The two-loop Higgs mass ($m_{h,2}$) as a function of the tree-level Higgs mass ($m_{h,0}$) for MI (left) and MII (right). Points satisfying all constraints for which $m_{\tilde{t}_1} < 2$ TeV are bright blue, paler points indicate low-energy constraints are satisfied and stop masses are in the range 2 TeV$< m_{\tilde{t}_1} < 2.3$ TeV, and points excluded by low energy constraints are shown in grey. The vertical line indicates the MSSM bound on $m_{h,0}$. The thick (thin) grey lines denote the central value (uncertainty) on m_h.

more sensitive determination however should be possible at the international linear collider (ILC), where for a centre of mass energy ($\sqrt{s}$) of 500 GeV, 500 fb^{-1} and polarized beams $P(e^+, e^-) = (-0.8, +0.3)$, a precision of 1.8% is quoted in Ref. [62].

In our model, the non-decoupled D-terms result in a tree level contribution to the Higgs coupling to down-type fermions. The ratio r_b ($= r_\tau$ at tree level) takes the form

$$r_b = -\frac{\sin\alpha}{\cos\beta}, \tag{5.3}$$

where α is the angle between the two Higgs doublets in the MSSM, and is defined by [9]

$$\tan 2\alpha = \frac{m_{A_0}^2 \cos 2\beta + m_{h,0}^2}{m_{A_0}^2 \cos 2\beta - m_{h,0}^2} \tan 2\beta. \tag{5.4}$$

Here m_{A_0} is the pseudoscalar Higgs mass of the MSSM and $m_{h,0}$ is the tree-level Higgs mass given in Eqn. (3.25). We plot the Higgs mass as a function of r_b in figure 6, where again the bright red points respect $m_{\tilde{t}_1} < 2$ TeV and all constraints imposed, the pale red points only satisfy low energy constraints (i.e. they do not comply with our requirements in the Higgs sector) and the grey points are excluded. We find that only a $\sim 2\%$ change in $r_{b/\tau}$ is required for MI, and a $\sim 4\%$ change for MII in order to obtain a Higgs mass of 125.5 GeV, with $m_{\tilde{t}_1} < 2$ TeV. Note that in our model, the enhanced coupling to down-type fermions results in a suppression of the signal strength μ_γ [4, 40], which was not favoured by initial measurements at the LHC [63]. However, as data has collected, the results for μ_γ appear more and more SM-like [60, 61]. As in this work the tree-level shift in the Higgs mass only needs to be under 10 GeV, we consider small values of $\Delta_{1,2}$, for which the deviation in the
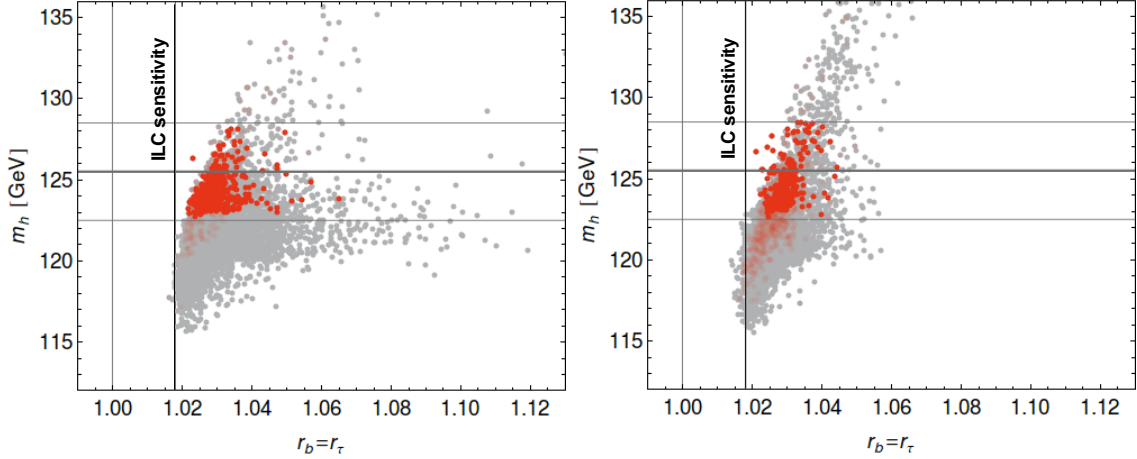
Figure 6. The Higgs mass as a function of $r_b = r_\tau$ for MI (left) and MII (right). Points satisfying all constraints and $m_{\tilde{t}_1} < 2$ TeV are bright red, whereas paler points indicate that stop masses are in the range $2\,\text{TeV} < m_{\tilde{t}_1} < 2.3$ TeV and only low-energy constraints are satisfied. Grey points are excluded. The thick (thin) grey horizontal lines denote the central value (uncertainty) on m_h and the vertical lines show the SM value $r_b = 1$ and the projected ILC uncertainty of 2% (see text).

coupling of the Higgs to down-type sfermions are well within the current LHC bounds (see e.g. Ref. [60]) as shown in figure 6. Such deviations should start to become detectable at the $\sqrt{s} = 500$ GeV ILC.

5.2 Sparticle searches at the LHC

As mentioned in section 4.2, the choice of Λ_3 ensures that the masses of the gluino and lower generation squarks approximately respect the limits from direct searches at the LHC. On the other hand, as the scale of the electroweak sector is set by $\Lambda_{1,2}$, by allowing $\Lambda_{1,2} < \Lambda_3$ we explore a range of parameter space for which the electroweak sector has a greater chance of being observed at the LHC. Further, as discussed previously, the quiver structure means that at the high scale the masses of uncoloured scalar particles lying on site A are suppressed, which can in particular result in light higgsinos or sleptons compared to minimal GMSB.

The phenomenology of the model depends decisively on the nature of the NLSP, as this decides which SM particle is present in the final state along with the gravitino $\tilde{G}$. ATLAS and CMS have recently made much progress on constraining gauge mediated models, where they study final states containing missing transverse energy (E_T^{miss}) due to the gravitino ($\tilde{G}$) escaping the detector. Bino-like NLSPs decay via $\tilde{\chi}_1 \to \tilde{G}\gamma$, such that the signature is $\gamma\gamma + E_T^{\text{miss}}$, along with additional jets depending on whether the production process is $\tilde{g}\tilde{g}$ or $\tilde{\chi}_1^0\tilde{\chi}_1^0$ [64]. When higgsino-like, the NLSP instead decays to a Higgs which can be detected via b jets, and a mixed higginos-bino NLSP can be searched for via a $\gamma b\bar{b} + E_T^{\text{miss}}$ signature [65]. For stau or sneutrino NLSPs the τ or ν must be searched for in the final state.
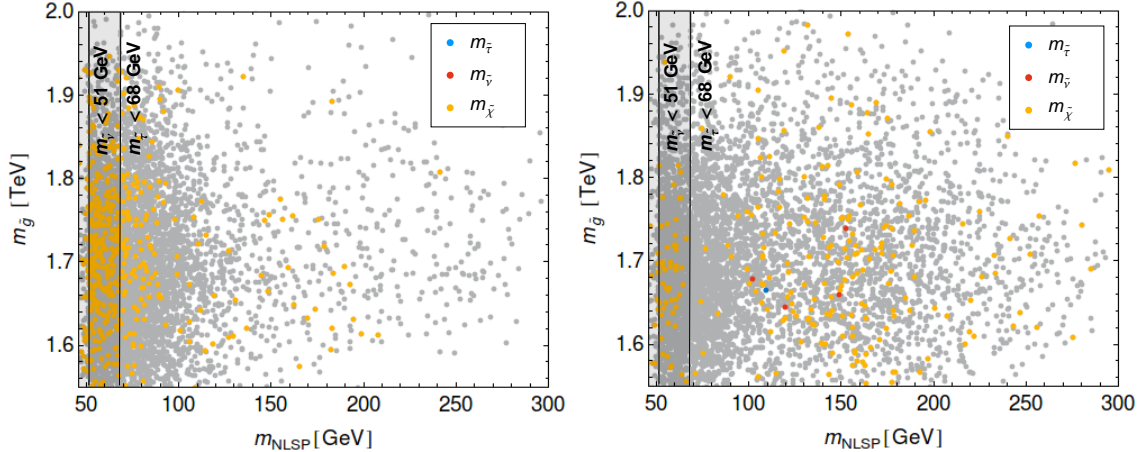
Figure 7. The gluino mass ($m_{\tilde{g}}$) as a function of NLSP mass (m_{NLSP}) for MI (left) and MII (right), where the colours indicate the type of NLSP as shown in the legend. The LEP exclusion limit for the case of the $\tilde{\tau}$ and $\tilde{\nu}$ NLSP is clearly marked, whereas the limit for $m_{\tilde{\chi}_1^0}$ is given by the y-axis. The grey points are excluded by experimental constraints as described in the text

In order to determine which experimental searches are relevant for these models, in figure 7 we examine the region of the $m_{\tilde{g}}$–m_{NLSP} plane accessed by our scans, indicating the type of NLSP for each point, which we find may be the neutralino, stau or sneutrino. The LEP exclusion limits (see section 4.2) for both the $\tilde{\tau}$ and $\tilde{\nu}$ NLSP are clearly marked, whereas the limit for $m_{\tilde{\chi}_1^0}$ is given by the y-axis. We find that for MII there are allowed points for which either the sneutrino or stau are the NLSP, however for MI no such points were found. In MI, the generations of sfermions are treated equally, such that the staus lie close to the other sleptons. On the other hand in the case of MII, as mentioned earlier, above symmetry breaking the third generation sfermions are on site A, whereas the lower generation ones on site B. This has the result that, as in the stop sector, the left-handed stau soft mass may be lower than the right-handed one, such that a sneutrino NLSP is possible. Therefore, although points in both models were found where the NLSP is the stau or sneutrino, only in MII do points survive the demanding constraints imposed on the Higgs mass and couplings due to measurements at the LHC, as illustrated in figure 8.

As the lightest neutralino $\tilde{\chi}_1^0$ appears to be the favoured candidate for the NLSP, it is interesting to explore its composition as this will enlighten us as to which decay modes are preferred. Therefore in figure 8, we show the lightest neutralino mass, $m_{\tilde{\chi}_1^0}$, as a function of M_1. From this plot one can deduce whether $\tilde{\chi}_1^0$ is higgsino or bino-like respectively, depending on the higgsino and bino masses, approximately given by μ and M_1 respectively. The ubiquitous blue points indicate $\mu > M_1$ whereas the more rare red points, which are even absent for MI, show $\mu < M_1$. The grey points are excluded by Higgs and low-energy constraints, and the horizontal line demarcates the LEP-excluded region for $m_{\tilde{\chi}_1^0}$. In both MI and MII, the higgsino is rarely lighter than the bino, such that the NLSP is mostly bino-like or mixed bino-higgsino, while both can easily be below 300 GeV. This is interesting in light of the fact that experiments are sensitive to the nature of the
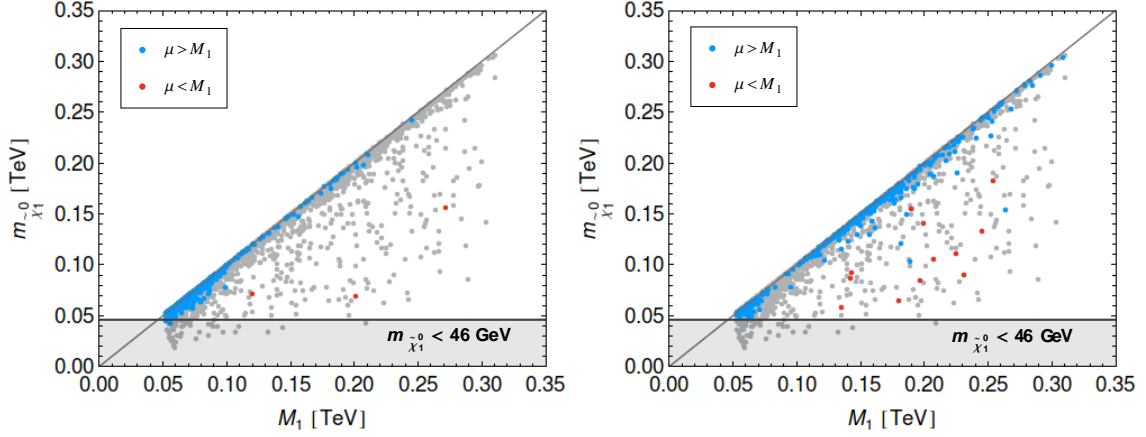
Figure 8. The lightest neutralino mass ($m_{\tilde{\chi}_1^0}$) as a function of M_1 for MI (left) and MII (right). The grey points are excluded by experimental constraints. The grey diagonal line indicates $m_{\tilde{\chi}_1^0} = M_1$, and the horizontal line indicates the LEP exclusion limit as described in the text.

neutralino NLSP, and the searches would therefore involve photons and/or Higgs bosons and missing transverse energy. Note that the feature of μ being light results in the model being less fine-tuned.

The experimental search strategy is not only dependent on the SM particle in the final state, but also on the decay length of the NLSP, $c\tau$. This can be approximated by [66],

$$c\tau \sim \frac{16\pi F^2}{m_{NLSP}^5},\tag{5.5}$$

where we take $F = \Lambda M$. In the region of parameter space considered in this paper, the NLSP decays within the detector. For the case of the neutralino NLSP decaying to a photon and gravitino, which is the prevalent case in both MI and MII, the excellent time measurement of the electromagnetic calorimeter in both ATLAS and CMS means that the time of arrival of the photon can be measured. If the NLSP decays immediately, i.e. if $c\tau < 10^{-4}$ m, then the decay is characterised as prompt, but otherwise it is non-prompt and it may be possible to deduce its decay length [67, 68]. We therefore show the decay length of the NLSP in figure 9, as a function of the mass m_{NLSP}. From this figure we can confirm that the lightest neutralino NLSP may undergo both promp or non-prompt decays to the photon and the gravitino, although in MI fewer points survive for which the neutralino decays promptly.

The most important channels for these models at the LHC are therefore searches for photons and missing transverse energy, where the photons may be prompt or non-prompt. Here the dominant production would be electroweak, as our choice of Λ_3 is such that the gluon and squark pair production is suppressed. Studies so far by CMS have concentrated on strong production of the bino-like NLSP [68, 69], whereas ATLAS has considered the diphoton and missing transverse energy final state from direct electroweakino production, for the case of both promptly decaying [64] and long-lived neutralinos [67]. However, the bounds obtained by ATLAS are not directly applicable here, as they are presented for a
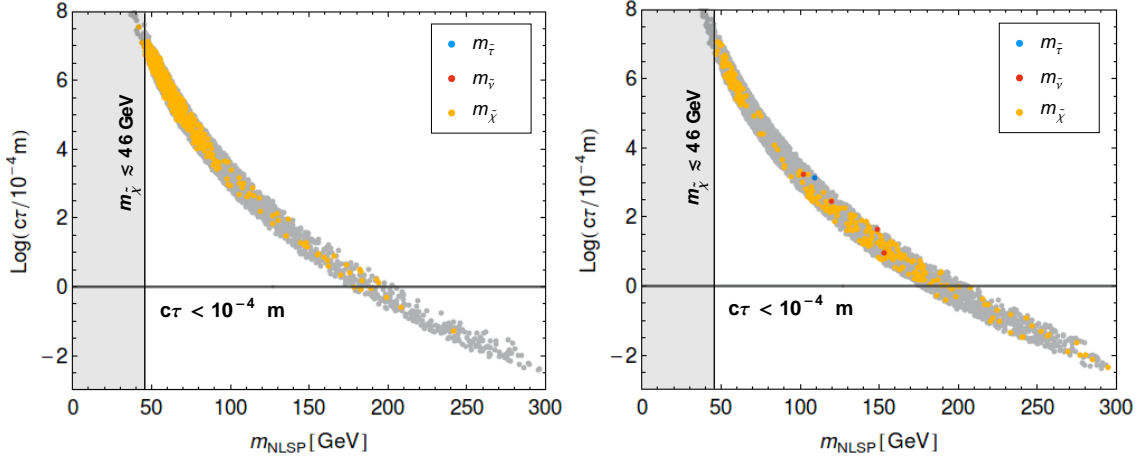
Figure 9. The decay length ($c\tau$) of the NLSP as a function of its mass (m_{NLSP}) for MI (left) and MII (right). Points for which $m_{\tilde{t}_1} < 2$ TeV and which satisfy all constraints imposed are shown in yellow, whereas the remaining excluded points are shown in grey. The vertical lines indicate the exclusion limits for staus and sneutrinos from LEP.

specific point SPS8 [70], where the neutralino NLSP decays predominantly to the photon and gravitino which is not necessarily the case in our model, especially due to the fact that the higgsino is often light. Therefore the bounds on final states including Higgs bosons, studied in Refs. [71, 72], must be taken into account. In order to constrain MII, one must further consider the stau and sneutrino NLSP, such that final states involving τs and missing transverse energy are of interest [72, 73]. It would be of great interest to combine all these excluded cross-sections to extract precise exclusion bounds (along the lines of e.g. Ref. [74]), but this is beyond the scope of this paper. It nonetheless seems that for gauge mediated models an interesting region of parameter space is starting to be probed, and we eagerly await further results.

6 Conclusions and discussion

In this paper we have examined phenomenological aspects of a minimal gauge extension of the MSSM containing two copies of the electroweak gauge group. Using state-of-the art publicly available HEP tools, we have computed the two-loop RG equations for *all* parameters of two variants MI and MII of this basic setup, characterised by different assignments for the representation of the MSSM chiral superfields. Although the model may be amenable to any set of soft term boundary conditions, we have chosen to work within the framework of gauge mediatied supersymmetry breaking and we performed the RG evolution from the messenger scale down to the electroweak scale in order to compute the sparticle spectrum. We calculated the corresponding sparticle masses at one loop, the predicted Higgs boson mass at two loops and further investigated the predictions of the models MI and MII for the most relevant experimental observables.

As the extended gauge structure results in non-decoupled D-terms which increase the tree-level Higgs mass, the resulting spectrum can be more natural than in minimal GMSB. We further found that in order to be in agreement with Higgs mass constraints, while keeping the stop masses below 2 TeV, one must generate sufficiently large Δ's (Eqn. (3.23)). This requires the linking soft mass m_L to be $\mathcal{O}(3-10)$ times higher than expected from the exact GMSB boundary conditions, which indicates a useful direction in which to extend this work on a theoretical level.

We also found that both variants MI and MII of the model would have interesting phenomenological consequences at colliders, since they could be probed either indirectly through Higgs couplings measurements or via direct sparticle production. The Higgs couplings to down-type fermions deviate from the SM due to the Δ's by $r_b \lesssim 6\%$ for MI and $r_b \lesssim 4\%$ for MII, and although at present this is well within experimental limits, such deviations should be measurable at a linear collider. As we have focused on the region of parameter space where the coloured sector is ~ 2 TeV in order to evade bounds on squark and gluino production from the LHC, while the electroweak sector is kept below 1 TeV, the most promising production channel at the LHC is the direct production of electroweakinos. As the predominant NLSP is the bino-like neutralino, diphoton and missing transverse energy searches offer the most promising search perspectives, though for MII, the NLSP is not limited to the bino such that finals states containing τ or h and missing transverse energy are also relevant. As the LHC exclusions are presented in terms of specific models, we are therefore keen to reinterpret these in order to understand how these bounds translate in the case of our model.

There are a number of ways in which this work may be extended. A first step, as mentioned earlier, would be to determine whether larger Δs can be realized without making m_L a free parameter by including $U(1)$ kinetic mixing or, more ambitiously, an additional $SU(3)$. This could be achieved by means of the tools we have developed with the help of the publicly available package `SARAH`. It would further be of interest to study related models of flavour, or models with chiral non-decoupled D-terms at the same level of precision. By moving Higgs fields or generations onto different quiver sites, such models are relatively straightforward to implement in our setup. It would also be ideal to construct single regime models, in particular for cases where the phenomenology of additional light states may become relevant. Furthermore, not only are there $SO(N)$ and $Sp(N)$ gauge extensions, but even more general quiver constructions, such as those with 3 or more sites [7, 75], may also be implemented in full. The study of these models and their GUT completion is also a noble task from the perspective of string phenomenology which has so far been rather neglected.

Acknowledgments

A Some further comments on the implementation

In this section we include some useful comments on the implementation of the model.

A.1 Fermion mixing and soft term matching

In regime 1 there are many fermions that may mix together. The uncharged fermions are the diagonal linking fermions, the light and massive bino-type fermions, the uncharged light and massive wino type fermions and finally the diagonal fermion of the A adjoint superfield as well as the K singlet fermion:

$$\left(\chi_L^1, \chi_{\tilde{L}}^1, \chi_L^4, \chi_{\tilde{L}}^4, \tilde{B}_L, \tilde{B}_M, \tilde{W}_L^3, \tilde{W}_M^3, \psi_A^1, \psi_K\right). \tag{A.1}$$

The lightest two of these states become the MSSM bino and uncharged wino. The mass matrices may be found in the .pdf of the model file in SARAH.

The charged fermions that mix together are the off-diagonal linking fermions, the charged wino-type light and massive gauginos and the off-diagonal A superfield fermions:

$$\left(\chi_L^2, \chi_{\tilde{L}}^2, \chi_L^3, \chi_{\tilde{L}}^3, \tilde{W}_L^1, \tilde{W}_M^1, \tilde{W}_L^2, \tilde{W}_M^2, \psi_A^2, \psi_A^3\right) \tag{A.2}$$

the lightest two of these become the MSSM charged winos. The rest of the states, both scalar and fermion, of the linking fields $K, A, L, \tilde{L}$ are integrated out at the threshold scale between the first and second regime.

A.2 MSSM Higgs and sfermion mixing matrices

The non-decoupled D-terms of section 3.4 appear in the tadpole equations as well as the Higgs mixing matrices. For the real components $(\phi_d, \phi_u), (\phi_d, \phi_u)$ we get

$$m_h^2 = \begin{pmatrix} m_{11} & -\frac{1}{4}g_{12}^2 v_d v_u - \mathrm{Re}[B_\mu] \\ -\frac{1}{4}g_{12}^2 v_d v_u - \mathrm{Re}[B_\mu] & m_{22} \end{pmatrix} \tag{A.3}$$

where $g_1 = g'$ and for convenience we use $g_{12}^2 = \left(g_1^2 + g_2^2 + g_1^2 \Delta_1^2 + g_2^2 \Delta_2^2\right)$.

$$m_{11} = \frac{1}{8}\left(8m_{H_d}^2 + 8|\mu|^2 + g_{12}^2\left(3v_d^2 - v_u^2\right)\right) \tag{A.4}$$

$$m_{22} = \frac{1}{8}\left(8m_{H_u}^2 + 8|\mu|^2 - g_{12}^2\left(-3v_u^2 + v_d^2\right)\right) \tag{A.5}$$

while for for pseudo-scalar Higgses $(\sigma_d, \sigma_u), (\sigma_d, \sigma_u)$ the relevant expressions are

$$m_{A^0}^2 = \begin{pmatrix} m_{11} & \mathrm{Re}[B_\mu] \\ \mathrm{Re}[B_\mu] & m_{22} \end{pmatrix} + \xi_Z m_Z^2 \tag{A.6}$$

$$m_{11} = \frac{1}{8}\left(8m_{H_d}^2 + 8|\mu|^2 + g_{12}^2\left(-v_u^2 + v_d^2\right)\right) \tag{A.7}$$

$$m_{22} = \frac{1}{8}\left(8m_{H_u}^2 + 8|\mu|^2 - g_{12}^2\left(-v_u^2 + v_d^2\right)\right) \tag{A.8}$$

The mass matrix for the charged Higgses $\left(H_d^-, H_u^{+,*}\right), \left(H_d^{-,*}, H_u^+\right)$ reads

$$m_{H^-}^2 = \begin{pmatrix} m_{11} & \frac{1}{4}\left(4B_\mu^* + \left(g_2^2 + g_2^2\Delta_2^2\right)v_dv_u\right) \\ \frac{1}{4}\left(4B_\mu + \left(g_2^2 + g_2^2\Delta_2^2\right)v_dv_u\right) & m_{22} \end{pmatrix} + \xi_{W^-}m_{W^-}^2 \tag{A.9}$$

$$m_{11} = \frac{1}{8}\left(8m_{H_d}^2 + 8|\mu|^2 + g_{12}^2v_d^2 + \hat{g}_{12}^2v_u^2\right) \tag{A.10}$$

$$m_{22} = \frac{1}{8}\left(8m_{H_u}^2 + 8|\mu|^2 + g_{12}^2v_u^2 + \hat{g}_{12}^2v_d^2\right) \tag{A.11}$$

where we have used the abbreviation $\hat{g}_{12}^2 = \left(-g_1^2 - g_1^2\Delta_1^2 + g_2^2 + g_2^2\Delta_2^2\right)$, and in all the above expressions, the ξ-terms are gauge-dependent contributions (and we work in Feynman gauge throughout this paper).

For completeness, we also include the mixing matrix $M_{\tilde{f}}$ of a generic sfermion $\tilde{f}$ which may be a squark or charged slepton. This matrix takes the form:

$$M_{\tilde{f}} = \begin{pmatrix} m_{\tilde{f}_L}^2 + m_f^2 + \hat{M}_Z^2(I_3^f - Q_f s_W^2) & m_f X_f^* \\ m_f X_f & m_{\tilde{f}_R}^2 + m_f^2 + \hat{M}_Z^2 Q_f s_W^2 \end{pmatrix}, \tag{A.12}$$

for $s_w = \sin\theta_W$ where θ_W is the Weinberg weak mixing angle, and we make use of the abbreviation $\hat{M}_Z^2 \equiv m_Z^2\cos 2\beta$. The off-diagonal element X_f is defined in terms of the trilinear coupling A_f via

$$X_f = A_f - \mu^*\{\cot\beta, \tan\beta\}, \tag{A.13}$$

where $\cot\beta$ applies for the up-type quarks, $f = u, c, t$, and $\tan\beta$ applies for the down-type fermions, $f = d, s, b, e, \mu, \tau$. Note that m_f, Q_f and I_3^f are the mass, charge and isospin projection of the fermion f, respectively. On diagonalization of this matrix one obtains the light and heavy sfermion masses $m_{\tilde{f}_1}$ and $m_{\tilde{f}_2}$.

A.3 Renormalisation group equations

We evolved the model down from the messenger scale M, to a threshold scale T_{scale}, which is associated with the masses of the linking field states $O(m_v^2)$. The two-loop renormalisation group equations were used in both regimes 1 and 2, along with one-loop finite energy corrections and two-loop anomalous dimensions.

The beta functions of the gauge couplings of the first regime at one loop are

$$\beta_{g_a} \equiv \frac{d}{dt}g_a = \frac{b_a}{16\pi^2}g_a^3 \quad \text{with} \quad b_a = (\frac{39}{5}, \frac{6}{5}, -2, 3, -3) \tag{A.14}$$

where $a = U(1)_A, U(1)_B, SU(2)_A, SU(2)_B, SU(3)$, which may be compared with the MSSM regime where

$$b_a = (33/5, 1, -3). \tag{A.15}$$

Let us also track the top Yukawas using the "only third family approximation",

$$\beta^1_{y_t} \equiv \frac{d}{dt} y_t \simeq \frac{y_t}{16\pi^2} \left[4y_t^* y_t + y_b^* y_b - \frac{16}{3} g_3^2 - 3g_{A2}^2 - \frac{13}{15} g_{A1}^2 \right]. \tag{A.16}$$

In the second regime these become

$$\beta_{y_t} \equiv \frac{d}{dt} y_t \simeq \frac{y_t}{16\pi^2} \left[6y_t^* y_t + y_b^* y_b - \frac{80}{15} g_3^2 - 3g_2^2 - \frac{13}{15} g_1^2 \right]. \tag{A.17}$$

In the first regime we find the trilinear A_t coupling to be

$$16\pi^2 \frac{d}{dt} A_t \simeq A_t \left[9y_t^* y_t + y_b^* y_b - \frac{16}{3} g_3^2 - 3g_{A2}^2 - \frac{13}{15} g_{A1}^2 \right]$$
$$+ y_t \left[\frac{32}{3} g_3^2 m_{\tilde{g}} + 6g_{A2}^2 m_{\tilde{W}_A} + \frac{26}{15} g_{A1}^2 m_{\tilde{B}_A} \right] + 2a_b y_b^* y_t \tag{A.18}$$

whereas in the MSSM

$$16\pi^2 \frac{d}{dt} A_t \simeq A_t \left[18y_t^* y_t + y_b^* y_b - \frac{16}{3} g_3^2 - 3g_2^2 - \frac{13}{15} g_1^2 \right]$$
$$+ y_t \left[\frac{32}{3} g_3^2 m_{\tilde{g}} + 6g_2^2 m_{\tilde{W}} + \frac{26}{15} g_1^2 m_{\tilde{B}} \right] + 2a_b y_b^* y_t. \tag{A.19}$$

Let us also look at how the gauginos obtain soft masses. The one-loop beta functions for the B-site gaugino soft masses are given by

$$\beta^1_{m_{\tilde{B}_B}} = \frac{12}{5} g_{B1}^2 m_{\tilde{B}_B} \quad \beta^1_{m_{\tilde{W}_B}} = -4g_{B2}^2 m_{\tilde{W}_B} \quad \beta^1_{m_{\tilde{g}}} = -6g_3^2 m_{\tilde{g}}. \tag{A.20}$$

For the A-site gauginos they are given by

$$\beta^1_{m_{\tilde{B}_A}} = \frac{78}{5} g_{A1}^2 m_{\tilde{B}_A} \quad \beta^1_{m_{\tilde{W}_A}} = 6g_{A2}^2 m_{\tilde{W}_A}. \tag{A.21}$$

Even though the A-site gaugino masses are vanishing at the messenger scale M the two loop-contributions which typically depend on all the other gaugino soft masses, feedback into the one-loop contributions. Finally the supersymmetric Dirac masses associated with the quiver structure will lift their mass eigenstates. The two-loop equations are given by

$$\beta^{(2)}_{m_{\tilde{B}_B}} = \frac{6}{25} g_{B1}^2 \left(12g_{B1}^2 m_{\tilde{B}_B} + 30g_{2A}^2 (m_{\tilde{W}_A} + m_{\tilde{W}_B}) + 30g_{B2}^2 (m_{\tilde{B}_B} + m_{\tilde{W}_B}) \right.$$
$$\left. + 6g_{A1}^2 (m_{\tilde{B}_A} + m_{\tilde{B}_B}) - 30Y_A^* (m_{\tilde{B}_B} Y_A - T_A) + 5Y_K^* (T_K - m_{\tilde{B}_B} Y_K) \right) \tag{A.22}$$

$$\beta^{(2)}_{m_{\tilde{B}_A}} = \frac{4}{75} g_{A1}^2 \left(-\frac{270}{2} Y_A^* (m_{\tilde{B}_A} Y_A - T_A) - \frac{45}{2} Y_K^* (m_{\tilde{B}_A} Y_K - T_K) + 620g_3^2 m_{\tilde{B}_A} \right.$$
$$+ 650g_{A1}^2 m_{\tilde{B}_A} + 315g_{A2}^2 m_{\tilde{B}_A} + 27g_{B1}^2 m_{\tilde{B}_A} + 135g_{B2}^2 m_{\tilde{B}_A} + 315g_{A2}^2 m_{\tilde{W}_A}$$
$$+ 27g_{B1}^2 m_{\tilde{B}_B} + 135g_{B2}^2 m_{\tilde{W}_B} + 620g_3^2 m_{\tilde{g}} \tag{A.23}$$
$$- 35m_{\tilde{B}_A} \text{Tr}(Y_d Y_d^\dagger) - 135m_{\tilde{B}_A} \text{Tr}(Y_e Y_e^\dagger) - 65m_{\tilde{B}_A} \text{Tr}(Y_u Y_u^\dagger)$$
$$\left. + 35\text{Tr}(Y_d^\dagger T_d) + 135\text{Tr}(Y_e^\dagger T_e) + 65\text{Tr}(Y_u^\dagger T_u) \right) \tag{A.24}$$

$$\beta^{(2)}_{m_{\tilde{W}_A}} = \frac{2}{5} g^2_{A2} \Big(15 g^2_{A1} m_{\tilde{B}_A} + 120 g^2_3 m_{\tilde{W}_A} + 15 g^2_{A1} m_{\tilde{W}_A} + 390 g^2_{A2} m_{\tilde{W}_A} + 6 g^2_{B1} m_{\tilde{W}_A}$$
$$+ 30 g^2_{B2} m_{\tilde{W}_A} + 6 g^2_{B1} m_{\tilde{B}_B} + 30 g^2_{B2} m_{\tilde{W}_B} + 120 g^2_3 m_{\tilde{g}}$$
$$- 30 Y^*_A (m_{\tilde{W}_A} Y_A - T_A) + Y^*_K (-5 m_{\tilde{W}_A} Y_K + 5 T_K)$$
$$- 10 m_{\tilde{W}_A} \mathrm{Tr}(Y_d Y_d^\dagger) - 10 m_{\tilde{W}_A} \mathrm{Tr}(Y_e Y_e^\dagger) - 10 m_{\tilde{W}_A} \mathrm{Tr}(Y_u Y_u^\dagger) + 10 \mathrm{Tr}(Y_d^\dagger T_d)$$
$$+ 10 \mathrm{Tr}(Y_e^\dagger T_e) + 10 \mathrm{Tr}(Y_u^\dagger T_u) \Big) \tag{A.25}$$

$$\beta^{(2)}_{m_{\tilde{W}_B}} = \frac{2}{5} g^2_{B2} \Big(6 g^2_{A1} m_{\tilde{B}_A} + 30 g^2_{A2} m_{\tilde{W}_A} + 6 g^2_{B1} m_{\tilde{B}_B} + 6 g^2_{A1} m_{\tilde{W}_B} + 30 g^2_{A2} m_{\tilde{W}_B}$$
$$+ 6 g^2_{B1} m_{\tilde{W}_B} + 140 g^2_{B2} m_{\tilde{W}_B} - 70 Y^*_A (m_{\tilde{W}_B} Y_A - T_A)$$
$$+ Y^*_K (-5 m_{\tilde{W}_B} Y_K + 5 T_K) \Big) \tag{A.26}$$

$$\beta^{(2)}_{m_{\tilde{g}}} = \frac{2}{15} g^2_3 \Big(33 g^2_{A1} m_{\tilde{B}_A} + 135 g^2_{A2} m_{\tilde{W}_A} + 420 g^2_3 m_{\tilde{g}} + 33 g^2_{A1} m_{\tilde{g}} + 135 g^2_{A2} m_{\tilde{g}}$$
$$- 20 m_{\tilde{g}} \mathrm{Tr}(Y_d Y_d^\dagger) - 20 m_{\tilde{g}} \mathrm{Tr}(Y_u Y_u^\dagger) + 20 \mathrm{Tr}(Y_d^\dagger T_d) + 20 \mathrm{Tr}(Y_u^\dagger T_u) \Big). \tag{A.27}$$

The soft masses for the quiver module run too:

$$\beta^{(1)}_{m^2_A} = -8 g^2_{B2} |m_{\tilde{W}_B}|^2 + 4(m^2_A + m^2_L + m^2_{\tilde{L}}) |Y_A|^2 + 4 |T_A|^2 \tag{A.28}$$

$$\beta^{(1)}_{m^2_K} = +2(m^2_K + m^2_L + m^2_{\tilde{L}}) |Y_K|^2 + 2 |T_K|^2 \tag{A.29}$$

$$\beta^{(1)}_{m^2_{\tilde{L}}} = \frac{1}{10} \Big(-12 g^2_{A1} |m_{\tilde{B}_A}|^2 - 60 g^2_{A2} |m_{\tilde{W}_A}|^2 - 12 g^2_{B1} |m_{\tilde{B}_B}|^2 - 60 g^2_{B2} |m_{\tilde{W}_B}|^2$$
$$+ 30(m^2_A + m^2_L + m^2_{\tilde{L}}) |Y_A|^2 + 5(m^2_K + m^2_L + m^2_{\tilde{L}}) |Y_K|^2$$
$$+ 30 |T_A|^2 + 5 |T_K|^2 + 6 g^2_{A1} \sigma_{1,3} \Big), \tag{A.30}$$

where by $\sigma_{1,3}$ we denote the soft mass combination

$$\sigma_{1,3} = -2\mathrm{Tr}(m^2_u) - 2 m^2_L + 2 m^2_{\tilde{L}} - m^2_{H_d} + m^2_{H_u} + \mathrm{Tr}(m^2_d)$$
$$+ \mathrm{Tr}(m^2_e) - \mathrm{Tr}(m^2_l) + \frac{1}{3} \mathrm{Tr}(m^2_q). \tag{A.31}$$

The vev of the linking fields runs as well:

$$\beta^{(1)}_v = \frac{v}{20} (-30 |Y_A| - 5 |Y_K| + 6 g^2_{A1} + 30 g^2_{A2} + 6 g^2_{B1} + 30 g^2_{B2}), \tag{A.32}$$

$$\beta^{(2)}_v = -\frac{v}{400} [+12(81 g^4_{A1} + 30 g^2_{A1} (g^2_{A2} + g^2_{B1} + g^2_{B2}) + 300 |Y_A|(8 g^2_{B2} - 1 |Y_K|)$$
$$- 2100 |Y_A|^4 + (225 g^4_{A2} + 15 g^4_{B1} + 30 g^2_{B1} g^2_{B2} + 30 g^2_{A2} (g^2_{B1}$$
$$+ 5 g^2_{B2}) - 25 g^4_{B2})) - 125 |Y_K|^4]. \tag{A.33}$$

Further equations may be found in the pdf for this model, including all anomalous dimensions and beta functions. At the electroweak scale one finds

$$|\mu|^2 = \frac{1}{8(v^2_d - v^2_u)} (-8 m^2_{H_d} v^2_d + 8 m^2_{H_u} v^2_u - g^2_1 \Delta^2_1 v^4_d - g^2_2 \Delta^2_2 v^4_d$$
$$+ g^2_1 \Delta^2_1 v^4_u + g^2_2 \Delta^2_2 v^4_u + g^2_2 v^4_u - g^2_2 v^4_d - g^2_1 v^4_d + g^2_1 v^4_u) \tag{A.34}$$

and

$$B_\mu = -\frac{v_d v_u}{4(v_d^2 - v_u^2)} \left(4m_{H_d}^2 - 4m_{H_u}^2 + (g_1^2 + g_2^2 + g_1^2 \Delta_1^2 + g_2^2 \Delta_2^2)(v_d^2 - v_u^2)\right). \tag{A.35}$$

which are after all used to minimise the electroweak tadpole equations.

A.4 Threshold effects

We integrate out various states at the threshold between the two regimes. These include the fermions discussed above as well as all linking scalars and scalars of K and A. To implement this correctly, with two-loop RGEs, we edited by hand the SPheno code to properly account for the finite shifts and the mass orderings of the particles integrated out, given by

$$g_i \to g_i \left[1 \pm \frac{g_i^2 b_{state}^i(R)}{8\pi^2} \ln\left(\frac{M_{state}}{M_T}\right)\right], \tag{A.36}$$

to account for our particular matter content and

$$m_{\tilde g} \to m_{\tilde g} \left[1 \pm \frac{g_i^2 b_{state}^i(R)}{8\pi^2} \ln\left(\frac{M_{state}}{M_T}\right)\right] \tag{A.37}$$

for the gluino shift between regimes. The other soft mass parameters for the bino and winos are matched as the lightest states as explained in appendix A.1. The shifts for each field component are given by

$$b_{state}(R) = \{11/3, -2/3, -1/3, -1/6\} \times \frac{T(R)}{D(R)}. \tag{A.38}$$

The numbers are associated to a gauge boson, weyl fermion, complex and real scalar respectively. $T(R)$ is the index (half the Dynkin index $I(R)$), such that $T(\Box) = 1/2, T(Adj) = N_c$). It is divided by the dimension of the representation D(R) as each shift is for the component of the field and not the full multiplet, in SARAH. The massive gauge fields are integrated out either on their own or by including them with the finite shifts of the real eaten goldstone modes.
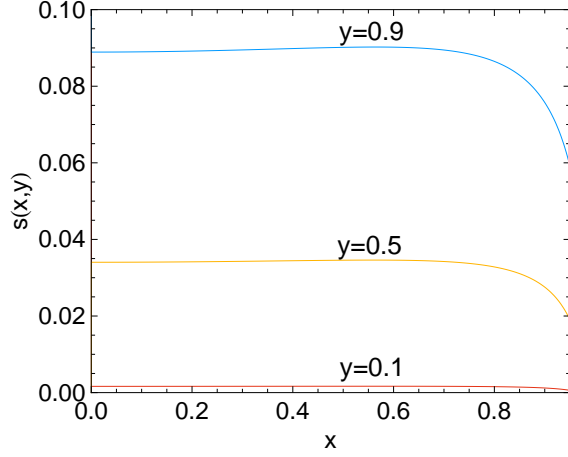
A.5 Soft mass function

In the SARAH package we included, in the form of a Fortran function, the generalisation of the usual mGMSB formula $f(x)$ to the case of a two site quiver model: $s(x,y)$. The analytic expression is given by

$$s(x,y) = \frac{1}{2x^2}\left(s_0 + \frac{s_1 + s_2}{y^2} + s_3 + s_4 + s_5\right) + (x \to -x), \tag{A.39}$$

where

$$s_0 = 2(1+x)\left(\log(1+x) - 2\text{Li}_2\left(\frac{x}{1+x}\right) + \frac{1}{2}\text{Li}_2\left(\frac{2x}{1+x}\right)\right),$$

$$s_1 = -4x^2 - 2x(1+x)\log^2(1+x) - x^2\,\text{Li}_2(x^2),$$

Figure 10. We show $s(x, y)$ as a function of the parameter x for fixed values of y as indicated.

$$s_2 = 8\,(1+x)^2\,h\left(\frac{y^2}{1+x}, 1\right) - 4x\,(1+x)\,h\left(\frac{y^2}{1+x}, \frac{1}{1+x}\right)$$

$$- 4xh\left(y^2, 1+x\right) - 8h\left(y^2, 1\right)\,,$$

$$s_3 = -2h\left(\frac{1}{y^2}, \frac{1}{y^2}\right) - 2x\,h\left(\frac{1+x}{y^2}, \frac{1}{y^2}\right) + 2(1+x)h\left(\frac{1+x}{y^2}, \frac{1+x}{y^2}\right)\,,$$

$$s_4 = (1+x)\left(2h\left(\frac{y^2}{1+x}, \frac{1}{1+x}\right) - h\left(\frac{y^2}{1+x}, 1\right) - h\left(\frac{y^2}{1+x}, \frac{1-x}{1+x}\right)\right)\,,$$

$$s_5 = 2h\left(y^2, 1+x\right) - 2h\left(y^2, 1\right)\,. \tag{A.40}$$

The function h is given by the integral

$$h(a, b) = \int_0^1 dx\left(1 + \text{Li}_2(1 - \mu^2) - \frac{\mu^2}{1 - \mu^2}\log\mu^2\right)\,. \tag{A.41}$$

The dilogarithm is defined as $\text{Li}_2(x) = -\int_0^1 \frac{dt}{t}\log(1 - xt)$ with

$$\mu^2 = \frac{ax + b(1 - x)}{x(1 - x)}\quad,\quad a = m_1^2/m_0^2\quad,\quad b = m_2^2/m_0^2. \tag{A.42}$$

So as not to introduce IR divergent pieces it is best to first evaluate terms with massless propagators. In that case the the function h simplifies to $h(0, b) = 1 + \text{Li}_2(1 - b)$ and has a symmetry $h(b, 0) = h(0, b)$. For four massive poles, the analytic expression for h is used in `SARAH`

$$h(a, b) = 1 - \frac{\log a \log b}{2} - \frac{a + b - 1}{\sqrt{\Delta}}\left(\text{Li}_2\left(-\frac{u_2}{v_1}\right) + \text{Li}_2\left(-\frac{v_2}{u_1}\right)\right.$$

$$\left. + \frac{1}{4}\log^2\frac{u_2}{v_1} + \frac{1}{4}\log^2\frac{v_2}{u_1} + \frac{1}{4}\log^2\frac{u_1}{v_1} - \frac{1}{4}\log^2\frac{u_2}{v_2} + \frac{\pi^2}{6}\right)\,, \tag{A.43}$$

where

$$\Delta = 1 - 2(a+b) + (a-b)^2 \,, \qquad u_{1,2} = \frac{1 + b - a \pm \sqrt{\Delta}}{2} \,, \tag{A.44}$$

$$v_{1,2} = \frac{1 - b + a \pm \sqrt{\Delta}}{2} \,. \tag{A.45}$$

References

[1] **ATLAS** Collaboration, G. Aad et al., *Observation of a new particle in the search for the Standard Model Higgs boson with the ATLAS detector at the LHC*, Phys.Lett. **B716** (2012) 1–29, [arXiv:1207.7214].

[2] **CMS** Collaboration, S. Chatrchyan et al., *Observation of a new boson at a mass of 125 GeV with the CMS experiment at the LHC*, Phys.Lett. **B716** (2012) 30–61, [arXiv:1207.7235].

[3] P. Batra, A. Delgado, D. E. Kaplan, and T. M. Tait, *The Higgs mass bound in gauge extensions of the minimal supersymmetric standard model*, JHEP **0402** (2004) 043, [hep-ph/0309149].

[4] K. Blum, R. T. D'Agnolo, and J. Fan, *Natural SUSY Predicts: Higgs Couplings*, JHEP **1301** (2013) 057, [arXiv:1206.5303].

[5] C. Csaki, J. Erlich, C. Grojean, and G. D. Kribs, *4-D constructions of supersymmetric extra dimensions and gaugino mediation*, Phys.Rev. **D65** (2002) 015003, [hep-ph/0106044].

[6] A. De Simone, J. Fan, M. Schmaltz, and W. Skiba, *Low-scale gaugino mediation, lots of leptons at the LHC*, Phys.Rev. **D78** (2008) 095010, [arXiv:0808.2052].

[7] M. McGarrie, *General Gauge Mediation and Deconstruction*, JHEP **1011** (2010) 152, [arXiv:1009.0012].

[8] N. Craig, D. Green, and A. Katz, *(De)Constructing a Natural and Flavorful Supersymmetric Standard Model*, JHEP **1107** (2011) 045, [arXiv:1103.3708].

[9] R. Auzzi, A. Giveon, S. B. Gudnason, and T. Shacham, *A Light Stop with Flavor in Natural SUSY*, JHEP **1301** (2013) 169, [arXiv:1208.6263].

[10] R. Huo, G. Lee, A. M. Thalapillil, and C. E. Wagner, $SU(2) \otimes SU(2)$ *Gauge Extensions of the MSSM Revisited*, Phys.Rev. **D87** (2013) 055011, [arXiv:1212.0560].

[11] R. T. D'Agnolo, E. Kuflik, and M. Zanetti, *Fitting the Higgs to Natural SUSY*, JHEP **1303** (2013) 043, [arXiv:1212.1165].

[12] M. McGarrie and R. Russo, *General Gauge Mediation in 5D*, Phys.Rev. **D82** (2010) 035001, [arXiv:1004.3305].

[13] A. Bharucha, A. Goudelis, and M. McGarrie, "Electroweak quiver gauge model." See supplementary material, October, 2013.

[14] R. Auzzi and A. Giveon, *The Sparticle spectrum in Minimal gaugino-Gauge Mediation*, JHEP **1010** (2010) 088, [arXiv:1009.1714].

[15] M. McGarrie, *Hybrid Gauge Mediation*, JHEP **1109** (2011) 138, [arXiv:1101.5158].

[16] A. Maloney, A. Pierce, and J. G. Wacker, *D-terms, unification, and the Higgs mass*, JHEP **0606** (2006) 034, [hep-ph/0409127].

[17] M. Drees, R. Godbole, and P. Roy, *Theory and phenomenology of sparticles: An account of four-dimensional N=1 supersymmetry in high energy physics*, .

[18] M. McGarrie, *5D Maximally Supersymmetric Yang-Mills in 4D Superspace: Applications*, *JHEP* **1304** (2013) 161, [arXiv:1303.4534].

[19] M. McGarrie and D. C. Thompson, *Warped General Gauge Mediation*, *Phys.Rev.* **D82** (2010) 125034, [arXiv:1009.4696].

[20] M. McGarrie, *Holography for General Gauge Mediation*, *JHEP* **1302** (2013) 132, [arXiv:1210.4935].

[21] F. Staub, *SARAH*, arXiv:0806.0538.

[22] F. Staub, *Automatic Calculation of supersymmetric Renormalization Group Equations and Self Energies*, *Comput.Phys.Commun.* **182** (2011) 808–833, [arXiv:1002.0840].

[23] F. Staub, *SARAH 3.2: Dirac Gauginos, UFO output, and more*, *Computer Physics Communications* **184** (2013) pp. 1792–1809, [arXiv:1207.0906].

[24] W. Porod, *SPheno, a program for calculating supersymmetric spectra, SUSY particle decays and SUSY particle production at e+ e- colliders*, *Comput.Phys.Commun.* **153** (2003) 275–315, [hep-ph/0301101].

[25] W. Porod and F. Staub, *SPheno 3.1: Extensions including flavour, CP-phases and models beyond the MSSM*, *Comput.Phys.Commun.* **183** (2012) 2458–2469, [arXiv:1104.1573].

[26] T. Hahn, *Generating Feynman diagrams and amplitudes with FeynArts 3*, *Comput.Phys.Commun.* **140** (2001) 418–431, [hep-ph/0012260].

[27] T. Hahn and C. Schappacher, *The Implementation of the minimal supersymmetric standard model in FeynArts and FormCalc*, *Comput.Phys.Commun.* **143** (2002) 54–68, [hep-ph/0105349].

[28] T. Hahn and M. Perez-Victoria, *Automatized one loop calculations in four-dimensions and D-dimensions*, *Comput.Phys.Commun.* **118** (1999) 153–165, [hep-ph/9807565].

[29] A. Pukhov, E. Boos, M. Dubinin, V. Edneral, V. Ilyin, et al., *CompHEP: A Package for evaluation of Feynman diagrams and integration over multiparticle phase space*, hep-ph/9908288.

[30] P. Bechtle, O. Brein, S. Heinemeyer, G. Weiglein, and K. E. Williams, *HiggsBounds: Confronting Arbitrary Higgs Sectors with Exclusion Bounds from LEP and the Tevatron*, *Comput.Phys.Commun.* **181** (2010) 138–167, [arXiv:0811.4169].

[31] P. Bechtle, O. Brein, S. Heinemeyer, G. Weiglein, and K. E. Williams, *HiggsBounds 2.0.0: Confronting Neutral and Charged Higgs Sector Predictions with Exclusion Bounds from LEP and the Tevatron*, *Comput.Phys.Commun.* **182** (2011) 2605–2631, [arXiv:1102.1898].

[32] P. Bechtle, O. Brein, S. Heinemeyer, O. Stal, T. Stefaniak, et al., *Recent Developments in HiggsBounds and a Preview of HiggsSignals*, *PoS* **CHARGED2012** (2012) 024, [arXiv:1301.2345].

[33] W. Kilian, T. Ohl, and J. Reuter, *WHIZARD: Simulating Multi-Particle Processes at LHC and ILC*, *Eur.Phys.J.* **C71** (2011) 1742, [arXiv:0708.4233].

[34] G. Belanger, F. Boudjema, A. Pukhov, and A. Semenov, *MicrOMEGAs 2.0: A Program to calculate the relic density of dark matter in a generic model*, *Comput.Phys.Commun.* **176** (2007) 367–382, [hep-ph/0607059].

[35] J. Camargo-Molina, B. O'Leary, W. Porod, and F. Staub, *Vevacious: A Tool For Finding The Global Minima Of One-Loop Effective Potentials With Many Scalars*, arXiv:1307.1477.

[36] G. Degrassi, P. Slavich, and F. Zwirner, *On the neutral Higgs boson masses in the MSSM for arbitrary stop mixing*, *Nucl.Phys.* **B611** (2001) 403–422, [hep-ph/0105096].

[37] A. Brignole, G. Degrassi, P. Slavich, and F. Zwirner, *On the O(alpha(t)**2) two loop corrections to the neutral Higgs boson masses in the MSSM*, *Nucl.Phys.* **B631** (2002) 195–218, [hep-ph/0112177].

[38] A. Brignole, G. Degrassi, P. Slavich, and F. Zwirner, *On the two loop sbottom corrections to the neutral Higgs boson masses in the MSSM*, *Nucl.Phys.* **B643** (2002) 79–92, [hep-ph/0206101].

[39] A. Dedes and P. Slavich, *Two loop corrections to radiative electroweak symmetry breaking in the MSSM*, *Nucl.Phys.* **B657** (2003) 333–354, [hep-ph/0212132].

[40] N. Craig and A. Katz, *A Supersymmetric Higgs Sector with Chiral D-terms*, *JHEP* **1305** (2013) 015, [arXiv:1212.2635].

[41] **ATLAS** Collaboration, *Physics at a High-Luminosity LHC with ATLAS*, arXiv:1307.7292.

[42] **CMS** Collaboration, *Projected Performance of an Upgraded CMS Detector at the LHC and HL-LHC: Contribution to the Snowmass Process*, arXiv:1307.7135.

[43] **CMS** Collaboration, S. Chatrchyan et al., *Observation of a new boson with mass near 125 GeV in pp collisions at sqrt(s) = 7 and 8 TeV*, *JHEP* **06** (2013) 081, [arXiv:1303.4571].

[44] G. Degrassi, S. Heinemeyer, W. Hollik, P. Slavich, and G. Weiglein, *Towards high precision predictions for the MSSM Higgs sector*, *Eur.Phys.J.* **C28** (2003) 133–143, [hep-ph/0212020].

[45] A. Arbey, M. Battaglia, A. Djouadi, and F. Mahmoudi, *The Higgs sector of the phenomenological MSSM in the light of the Higgs boson discovery*, *JHEP* **1209** (2012) 107, [arXiv:1207.1348].

[46] **Particle Data Group** Collaboration, J. Beringer et al., *Review of Particle Physics (RPP)*, *Phys.Rev.* **D86** (2012) 010001.

[47] **ATLAS** Collaboration, *Search for squarks and gluinos with the atlas detector in final states with jets and missing transverse momentum and 20.3 fb^{-1} of $\sqrt{s}$ = 8 tev proton-proton collision data*, Tech. Rep. ATLAS-CONF-2013-047, CERN, Geneva, May, 2013.

[48] **CMS** Collaboration, S. Chatrchyan et al., *Search for new physics in the multijet and missing transverse momentum final state in proton-proton collisions at $\sqrt{s}$ = 7 TeV*, *Phys.Rev.Lett.* **109** (2012) 171803, [arXiv:1207.1898].

[49] H. Baer, V. Barger, and D. Mickelson, *How conventional measures overestimate electroweak fine-tuning in supersymmetric theory*, arXiv:1309.2984.

[50] **ALEPH, DELPHI, L3 and OPAL** Collaboration, LEPSUSYWG, *notes LEPSUSYWG/02-04.1 and LEPSUSYWG/01-03.1*, 2001.

[51] **ALEPH** Collaboration, R. Barate et al., *Search for gauge mediated SUSY breaking topologies at $S^{(1/2)}$ similar to 189-GeV*, *Eur.Phys.J.* **C16** (2000) 71–85.

[52] **ALEPH** Collaboration, R. Barate et al., *Search for supersymmetric particles in e^+e^- collisions at $\sqrt{s}$ up to 202-GeV and mass limit for the lightest neutralino*, *Phys.Lett.* **B499** (2001) 67–84, [hep-ex/0011047].

[53] **ALEPH** Collaboration, D. Decamp et al., *Searches for new particles in Z decays using the ALEPH detector*, *Phys.Rept.* **216** (1992) 253–340.

[54] P. Bechtle, S. Heinemeyer, O. Stål, T. Stefaniak, and G. Weiglein, *HiggsSignals: Confronting arbitrary Higgs sectors with measurements at the Tevatron and the LHC*, `arXiv:1305.1933`.

[55] **Heavy Flavor Averaging Group** Collaboration, Y. Amhis et al., *Averages of B-Hadron, C-Hadron, and tau-lepton properties as of early 2012*, `arXiv:1207.1158`.

[56] **LHCb** Collaboration, R. Aaij et al., *First Evidence for the Decay $B_s^0 \to \mu^+\mu^-$*, *Phys.Rev.Lett.* **110** (2013) 021801, [`arXiv:1211.2674`].

[57] H. E. Haber, R. Hempfling, and A. H. Hoang, *Approximating the radiatively corrected Higgs mass in the minimal supersymmetric model*, *Z.Phys.* **C75** (1997) 539–554, [`hep-ph/9609331`].

[58] R. Benbrik, M. Gomez Bock, S. Heinemeyer, O. Stal, G. Weiglein, et al., *Confronting the MSSM and the NMSSM with the Discovery of a Signal in the two Photon Channel at the LHC*, *Eur.Phys.J.* **C72** (2012) 2171, [`arXiv:1207.1096`].

[59] P. Bechtle, S. Heinemeyer, O. Stal, T. Stefaniak, G. Weiglein, et al., *MSSM Interpretations of the LHC Discovery: Light or Heavy Higgs?*, *Eur.Phys.J.* **C73** (2013) 2354, [`arXiv:1211.1955`].

[60] **ATLAS** Collaboration, G. Aad et al., *Measurements of Higgs boson production and couplings in diboson final states with the ATLAS detector at the LHC*, *Phys.Lett.* **B** (2013) [`arXiv:1307.1427`].

[61] **CMS** Collaboration, *Combination of standard model Higgs boson searches and measurements of the properties of the new boson with a mass near 125 GeV*, Tech. Rep. CMS-PAS-HIG-12-045, CERN, Geneva, 2012.

[62] H. Baer, T. Barklow, K. Fujii, Y. Gao, A. Hoang, et al., *The International Linear Collider Technical Design Report - Volume 2: Physics*, `arXiv:1306.6352`.

[63] **ATLAS** Collaboration, *Coupling properties of the new Higgs-like boson observed with the ATLAS detector at the LHC*, Tech. Rep. ATLAS-CONF-2012-127, ATLAS-COM-CONF-2012-161, CERN, Geneva, 2012.

[64] **ATLAS** Collaboration, G. Aad et al., *Search for diphoton events with large missing transverse momentum in 7 TeV proton-proton collision data with the ATLAS detector*, *Phys.Lett.* **B718** (2012) 411–430, [`arXiv:1209.0753`].

[65] **ATLAS** Collaboration, G. Aad et al., *Search for supersymmetry in events with photons, bottom quarks, and missing transverse momentum in proton-proton collisions at a centre-of-mass energy of 7 TeV with the ATLAS detector*, *Phys.Lett.* **B719** (2013) 261–279, [`arXiv:1211.1167`].

[66] G. Giudice and R. Rattazzi, *Theories with gauge mediated supersymmetry breaking*, *Phys.Rept.* **322** (1999) 419–499, [`hep-ph/9801271`].

[67] **ATLAS** Collaboration, G. Aad et al., *Search for non-pointing photons in the diphoton and $E_T^m iss$ final state in sqrt(s) = 7 TeV proton-proton collisions using the ATLAS detector*, *Phys.Rev.* **D88** (2013) 012001, [`arXiv:1304.6310`].

[68] **CMS** Collaboration, S. Chatrchyan et al., *Search for long-lived particles decaying to photons and missing energy in proton-proton collisions at $\sqrt{s} = 7$ TeV*, *Phys.Lett.* **B722** (2013) 273–294, [`arXiv:1212.1838`].

[69] **CMS** Collaboration, S. Chatrchyan et al., *Search for new physics in events with photons, jets, and missing transverse energy in pp collisions at $\sqrt{s} = 7$ TeV*, JHEP **1303** (2013) 111, [arXiv:1211.4784].

[70] B. Allanach, M. Battaglia, G. Blair, M. S. Carena, A. De Roeck, et al., *The Snowmass points and slopes: Benchmarks for SUSY searches*, Eur.Phys.J. **C25** (2002) 113–123, [hep-ph/0202233].

[71] **ATLAS** Collaboration, *Search for supersymmetry in final states with jets, missing transverse momentum and a Z boson at $\sqrt{s} = 8$ TeV with the ATLAS detector*, Tech. Rep. ATLAS-CONF-2012-152, CERN, Geneva, Nov, 2012.

[72] **CMS** Collaboration, *A search for anomalous production of events with three or more leptons using 19.5/fb of sqrt(s)=8 TeV LHC data*, Tech. Rep. CMS-PAS-SUS-13-002, CERN, Geneva, 2013.

[73] **ATLAS** Collaboration, *Search for Supersymmetry in Events with Large Missing Transverse Momentum, Jets, and at Least One Tau Lepton in 21 fb^{-1} of $\sqrt{s} = 8$ TeV Proton-Proton Collision Data with the ATLAS Detector*, Tech. Rep. ATLAS-CONF-2013-026, CERN, Geneva, Mar, 2013.

[74] A. Bharucha, S. Heinemeyer, and F. von der Pahlen, *Direct Chargino-Neutralino Production at the LHC: Interpreting the Exclusion Limits in the Complex MSSM*, arXiv:1307.4237.

[75] R. Auzzi, A. Giveon, and S. B. Gudnason, *Mediation of Supersymmetry Breaking in Quivers*, JHEP **1112** (2011) 016, [arXiv:1110.1453].